Monthly Notices
of the
ROYAL ASTRONOMICAL SOCIETY

Mon. Not. R. Astron. Soc. **420,** 1462–1480 (2012) doi:10.1111/j.1365-2966.2011.20134.x

Toward ensemble asteroseismology of ZZ Ceti stars with fully evolutionary models

A. D. Romero,[1,2] A. H. Córsico,[1,2]★ L. G. Althaus,[1,2] S. O. Kepler,[3] B. G. Castanheira[3,4] and M. M. Miller Bertolami[1,2]

[1]*Facultad de Ciencias Astronómicas y Geofísicas, Universidad Nacional de La Plata, La Plata 1900, Argentina*
[2]*CONICET, Consejo Nacional de Investigaciones Científicas y Técnicas, Argentina*
[3]*Departamento de Astronomia, Universidade Federal do Rio Grande do Sul, Av. Bento Goncalves 9500, Porto Alegre 91501-970, RS, Brazil*
[4]*Institut für Astronomie, Türkenschanzstr. 17, A-1180 Wien, Austria*

Accepted 2011 November 3. Received 2011 November 2; in original form 2011 September 29

ABSTRACT

ZZ Ceti stars form the most numerous group of degenerate variable stars. They are otherwise normal DA (H-rich atmospheres) white dwarfs that exhibit pulsations. Here, we present an asteroseismological analysis for 44 bright ZZ Ceti stars based on a new set of fully evolutionary DA white dwarf models characterized by detailed chemical profiles from the centre to the surface. One of our targets is the archetypal ZZ Ceti star G117−B15A, for which we obtain an asteroseismological model with an effective temperature and a surface gravity in excellent agreement with the spectroscopy. The asteroseismological analysis of a set of 44 ZZ Ceti stars has the potential to characterize the global properties of the class, in particular the thicknesses of the hydrogen envelope and the stellar masses. Our results support the belief that white dwarfs in the solar neighbourhood harbour a broad range of hydrogen-layer thickness.

Key words: astroseismology – stars: evolution – stars: individual: ZZ Ceti stars – stars: interiors – stars: oscillations – white dwarfs.

1 INTRODUCTION

Pulsating DA (H-rich atmospheres) white dwarfs, commonly known as ZZ Ceti or DAV variable stars, comprise the most numerous class of compact pulsators. They are located in a narrow and probably pure instability strip with effective temperatures between 10 500 and 12 500 K (e.g. Fontaine & Brassard 2008; Winget & Kepler 2008; Althaus et al. 2010a). ZZ Ceti stars are characterized by multimode photometric variations of up to 0.30 mag caused by non-radial g-mode pulsations of low degree ($\ell \leq 2$) and periods between 70 and 1500 s. The driving mechanism thought to excite the pulsations is a sort of combination of the κ–γ mechanism acting in the hydrogen partial ionization zone (Dolez & Vauclair 1981; Winget et al. 1982) and the 'convective driving' mechanism proposed first by Brickhill (1991) and later re-examined by Goldreich & Wu (1999). The later mechanism is supposed to be dominant once a thick convection zone has developed at the stellar surface.

White dwarf asteroseismology fully exploits the comparison between the observed pulsation periods in white dwarfs and the periods computed for appropriate theoretical models. It allows us to infer details of the origin, internal structure and evolution of white dwarfs (Fontaine & Brassard 2008; Winget & Kepler 2008; Althaus et al. 2010a). In particular, constraints on the stellar mass, the thickness of the outer envelopes, the core chemical composition, weak magnetic fields and slow rotation rates can be inferred from the observed period patterns of ZZ Ceti stars. In addition, asteroseismology of ZZ Ceti stars is a valuable tool for studying axions (Isern, Hernanz & García-Berro 1992; Córsico et al. 2001, 2011; Bischoff-Kim, Montgomery & Winget 2008b; Isern et al. 2010), crystallization (Montgomery & Winget 1999; Córsico et al. 2004, 2005; Metcalfe, Montgomery & Kanaan 2004; Kanaan et al. 2005) and important properties of the outer convection zones (Montgomery 2005a,b, 2007). Finally, the temporal changes in the observed stable periods allow the measurement of the white dwarf evolutionary time-scale and the detection possible planets orbiting white dwarfs (Mullally et al. 2008).

Among the numerous ZZ Ceti stars currently known (148 stars; Castanheira et al. 2010), in this paper we will analyse 44 bright ZZ Ceti stars which are listed in table 1 of Fontaine & Brassard (2008). We defer to a future work the study of the fainter ZZ Ceti stars discovered within the Sloan Digital Sky Survey (SDSS; Mukadam et al. 2004; Kepler et al. 2005b; Mullally et al. 2005; Castanheira et al. 2006, 2007, 2010). The first target star of our seismological survey is the most studied member of the class, the paradigmatic star G117−B15A. This star is an otherwise typical DA white dwarf, the variability of which was discovered by McGraw & Robinson (1976) and, since then, it has been monitored continuously. The surface gravity, total mass and effective

★E-mail: acorsico@fcaglp.unlp.edu.ar

temperature of this star have been the subject of numerous spectroscopic determinations. For instance, values of $\log g = 7.97 \pm 0.05$, $M_* = 0.59 \pm 0.03\,\mathrm{M}_\odot$ and $T_{\rm eff} = 11\,630 \pm 200$ K have been derived by Bergeron, Wesemael & Beauchamp (1995a) and Bergeron et al. (2004) from optical spectra. Koester & Allard (2000) have reported somewhat lower values for the gravity and mass, $\log g = 7.86 \pm 0.14$, $M_* = 0.53 \pm 0.07\,\mathrm{M}_\odot$ and a higher effective temperature, $T_{\rm eff} = 11\,900 \pm 140$ K, from *Hubble Space Telescope* (*HST*) ultraviolet (UV) spectra. G117−B15A has oscillation periods Π (amplitudes A) of 215.20 s (17.36 mma), 270.46 s (6.14 mma) and 304.05 s (7.48 mma; Kepler et al. 1982) that correspond to genuine pulsation modes. The star also shows the harmonic of the largest amplitude mode and two linear combinations. Kepler et al. (2005a) used the rate of change of the 215 s periodicity to show that the star has a C–O core. The first detailed asteroseismological study of this star was presented by Bradley (1998). This author obtained two different structures for the star according to the assignation of the radial order (k) of the modes exhibited by the star. If the periods at 215, 271 and 304 s are associated with $k = 1, 2, 3$, respectively, this author obtained an asteroseismological model with a hydrogen envelope mass $M_{\rm H}/M_* \sim 3 \times 10^{-7}$. If, instead, the periods have $k = 2, 3, 4$, the asteroseismological model was characterized by $M_{\rm H}/M_* \sim 1.5 \times 10^{-4}$. Note that there are three orders of magnitude of difference in the mass of the H envelope between the two possible (and nearly equally valid within their models) asteroseismological solutions. A similar degeneracy of seismological solutions for G117−B15A was also found by Benvenuto et al. (2002) on the basis of independent stellar and pulsation modelling. More recently, Castanheira & Kepler (2008) have found a seismological solution with $M_{\rm H}/M_* \sim 10^{-7}$ and $k = 1, 2, 3$ and another equally valid solution with $M_{\rm H}/M_* \sim 10^{-5}$ and $k = 2, 3, 4$. Finally, Bischoff-Kim, Montgomery & Winget (2008a) also found two classes of solutions, one characterized by 'thin' H envelopes, and other associated with 'thick' H envelopes, although their 'thick' envelope solutions ($M_{\rm H}/M_* = 6 \times 10^{-7}$) are considerably thinner than those of the previous works.

Each of the mentioned asteroseismological studies constitutes a clear demonstration of the formidable capability of asteroseismology to shed light on the internal structure of DA white dwarfs. However, as important as they are, all of these studies are based on DA white dwarf models that lack a fully consistent assessment of the internal chemical structure from the core to the outer layers. For instance, in the models of Bradley (1998), although the C/He and He/H chemical interfaces are more realistic than previous studies that used the trace element approximation (Tassoul, Fontaine & Winget 1990), the core C–O chemical profiles have a (unrealistic) ramp-like shape. In the case of Benvenuto et al. (2002), the artificially generated models are characterized by He/H chemical interfaces resulting from a time-dependent element diffusion treatment, and the C–O core chemical structure is extracted from the independent computations of Salaris et al. (1997). So, there is no consistent coupling between the chemical structure of the core and the chemical stratification of the envelope of the models. On the other hand, the recent works by Castanheira & Kepler (2008, 2009) are based on DA white dwarf models similar to those of Bradley (1998), with a parametrization that mimics the results of time-dependent diffusion computations for the He/H chemical interfaces, but with a simplified treatment of the core chemical structure (50 per cent O and 50 per cent C). Finally, the study of Bischoff-Kim et al. (2008a) employs DA white dwarf models similar to those of Castanheira & Kepler (2008, 2009), but the envelope is stitched to a core that incorporates chemical profiles similar to those of Salaris et al. (1997).

Needless to say, white dwarf stellar models with consistent and detailed chemical profiles *from the centre to the surface* are needed to correctly assess the adiabatic pulsation periods and also the mode-trapping properties of the DAVs, the crucial aspects of white dwarf asteroseismology (Bradley 1996; Córsico et al. 2002). In this regard, Althaus et al. (2010b) (see also Renedo et al. 2010) have recently presented the first complete set of DA white dwarf models with consistent chemical profiles for both the core *and* the envelope for various stellar masses appropriate for detailed asteroseismological fits of ZZ Ceti stars. These chemical profiles are computed from the full and complete evolution of the progenitor stars from the zero-age main sequence (ZAMS), through the thermally pulsing and mass-loss phases on the asymptotic giant branch (AGB), and from time-dependent element diffusion predictions during the white dwarf stage.

In this paper, we carry out the first asteroseismological application of the DA white dwarf models presented in Althaus et al. (2010b). Specifically, we perform a detailed asteroseismological study on 44 ZZ Ceti stars that includes the archetypal star G117−B15A, by using a grid of new evolutionary models characterized by consistent chemical profiles and covering a wide range of stellar masses, thicknesses of the hydrogen envelope and effective temperatures. The asteroseismological analysis of such a large set of stars is a good starting point for ensemble asteroseismology of ZZ Ceti stars (see Castanheira & Kepler 2009). We also explore, in the frame of standard evolutionary calculations for the formation of DA white dwarfs, to what extent the mass of the He-rich envelope ($M_{\rm He}$) expected in DA white dwarfs depends on the details of prior evolution of progenitor stars. The paper is organized as follows. In Section 2, we provide a brief description of the evolutionary code, the input physics adopted in our calculations and the grid of models employed. There, we also explore the dependence of $M_{\rm He}$ on the progenitor evolution. In Section 3, we describe our asteroseismological procedure. In Section 4, we present our results, starting with the asteroseismological analysis for G117−B15A and a comparison with previous results (Section 4.2), and then by describing the results for the set of 44 stars (Section 4.3). We conclude in Section 5 by summarizing our findings.

2 NUMERICAL TOOLS AND MODELS

2.1 Evolutionary code and input physics

The present asteroseismological study is based on the full DA white dwarf evolutionary models of Althaus et al. (2010b) (see also Renedo et al. 2010) generated with the LPCODE evolutionary code. In Fig. 1 we depict the grid of DA white dwarf sequences considered in this study. To our knowledge, these models are the first complete set of DA white dwarfs models characterized by consistent chemical profiles for both the core and envelope. This feature renders these models particularly suitable for asteroseismological studies of DA white dwarfs.

Here, we will briefly outline the most relevant characteristics of our evolutionary models of relevance for their pulsation properties. Further details can be found in Althaus et al. (2010b). In our computations, the $^{12}\mathrm{C}(\alpha, \gamma)^{16}\mathrm{O}$ reaction rate, of special relevance for the C–O stratification of the emerging white dwarf, is taken from Angulo et al. (1999). Thus, our white dwarf models are characterized by systematically lower central O abundances than the

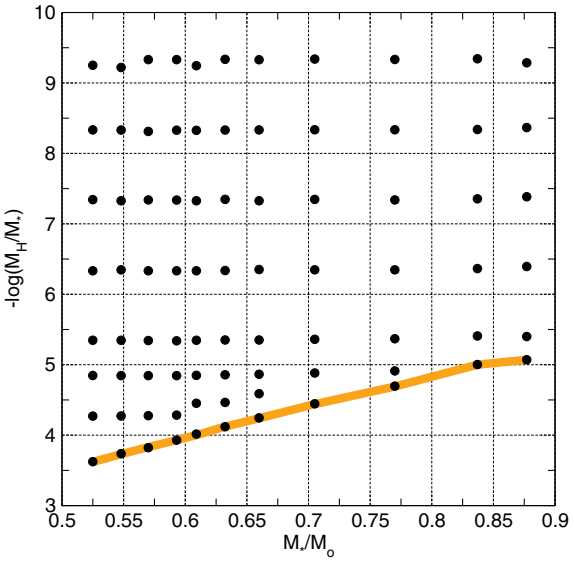

Figure 1. The grid of DA white dwarf evolutionary sequences considered in this study represented in the plane M_*–log (M_H/M_*). Each small circle corresponds to a sequence of DA white dwarf models with a given stellar mass and thickness of H envelope. The circles connected with a thick (orange) line correspond to the values of the maximum thickness of the H envelope as predicted by our evolutionary computations. For each sequence, we have pulsationally analysed about 200 stellar models covering the effective temperature range of 14 000–9000 K.

values predicted by Salaris et al. (1997), who used the larger rate of Caughlan et al. (1985). For example, for a ∼0.61 $M_\odot$ white dwarf, our computations give $X_O \sim 0.73$, about 4 per cent lower than quoted by Salaris et al. (1997) ($X_O \sim 0.76$). Extra-mixing episodes during core He burning, of relevance for the final chemical stratification of white dwarfs (Straniero et al. 2003), was allowed to occur following the prescription of Herwig et al. (1997). Breathing pulses, which are convective runaways occurring towards the end of core helium burning, were suppressed. An important feature of our computations is that extra-mixing episodes were disregarded during the thermally pulsing AGB phase, in line with theoretical and observational evidence (Lugaro et al. 2003; Herwig et al. 2007; Salaris et al. 2009). This leads to the inhibition of the occurrence of the third dredge-up in low-mass stars, and consequently, to the gradual increase in the hydrogen-free core (HFC) mass as evolution proceeds during this phase. As a result, the initial-final mass relationship by the end of the thermally pulsing AGB is markedly different from that resulting from considering the mass of the HFC right before the first thermal pulse. This issue is relevant for the C–O composition expected in a white dwarf. Depending on the white dwarf mass, the central oxygen abundance may be underestimated by about 15 per cent if it is assumed that the white dwarf mass is the HFC mass by the first thermal pulse (see Althaus et al. 2010b).

We considered mass-loss episodes during the core helium burning stage and on the red giant branch following Schröder & Cuntz (2005). During the AGB and thermally pulsing AGB phases, we adopted the maximum mass-loss rate between the prescription of Schröder & Cuntz (2005) and that of Vassiliadis & Wood (1993).

In our evolutionary computations, we have considered the distinct physical processes that are responsible for changes in the chemical abundance distribution during white dwarf evolution. This is one of the most important improvements of our computations in comparison with previous asteroseismological works on DA white dwarfs. In particular, element diffusion strongly modifies the chemical composition profile throughout their outer layers in the course of evolution. As a result of diffusion processes, our sequences develop pure H envelopes and modifies the various intershells above the C–O core. We have considered gravitational settling as well as thermal and chemical diffusion – but not radiative levitation, which is relevant at high effective temperatures for determining the surface composition – of ^{1}H, ^{3}He, ^{4}He, ^{12}C, ^{13}C, ^{14}N and ^{16}O (see Althaus et al. 2003, for details). The standard mixing length theory for convection – with the free parameter $\alpha = 1.61$ – has been adopted. Our treatment of time-dependent diffusion is based on the multicomponent gas treatment presented in Burgers (1969). In LPCODE, diffusion becomes operative once the wind limit is reached at high effective temperatures (Unglaub & Bues 2000). In addition, abundance changes resulting from residual nuclear burning have been taken into account in our simulations. Finally, we considered the chemical rehomogenization of the inner carbon–oxygen profile induced by Rayleigh–Taylor (RT) instabilities following Salaris et al. (1997).

An important feature of our models is the dependence on the stellar mass of the outer layer chemical stratification expected in ZZ Ceti stars. Indeed, for the more massive models, diffusion strongly modifies the chemical abundance distribution, eroding the thick intershell region below the He buffer by the time evolution has reached the domain of the ZZ Ceti instability strip (see Althaus et al. 2010b). This is in contrast with the situation encountered in our less massive models ($M_* \lesssim 0.63\,M_\odot$), where the intershell region is not removed by diffusion. This is because element diffusion is less efficient in less massive models (with the subsequent longer diffusion time-scale) and also because the intershell is thicker in these models. Regarding white dwarf asteroseismology, these are not minor issues, since the presence of a double-layered structure in the helium-rich layers is expected to affect the theoretical g-mode period spectra of ZZ Ceti stars. It is clear that white dwarf evolution computed in a consistent way with element diffusion as considered in this study is required for precise asteroseismology.

2.2 About the He content of a DA white dwarf star

In this section we show that, in the frame of standard evolutionary computations for the formation of DA white dwarfs, the He content of these stars cannot be substantially smaller than that predicted by our calculations. To do this, we compute the evolution of a 2 $M_\odot$ star from the ZAMS until the thermally pulsing phase on the AGB. The only way we envisage in which the star may experience a substantial decrease in its content of He is by undergoing a large number of thermal pulses. In order for the model star to experience the largest possible number of thermal pulses, and thus, the content of He decreases as much as possible, we switched off mass loss during this stage in our evolutionary code. The results of this experiment are depicted in Fig. 2, in which we show the He content in the region limited by the boundaries of the He-free core (HeFC) and the HFC in terms of time during the thermally pulsing phase (upper panel), and the surface luminosity and the H- and He-burning luminosities for each pulse in that phase (lower panel). We stopped the experiment when the object experienced about 30 thermal pulses, which is enough for our purposes. We found that the He content of the object decreased from $M_{He}/M_\odot = 3.34 \times 10^{-2}$ (before the first thermal pulse) to $M_{He}/M_\odot = 8.6 \times 10^{-3}$ (before the thirtieth thermal pulse). Thus, the decrease (in solar masses) of the He content of the HFC is of a factor 3.89. However, it should be kept in mind that this

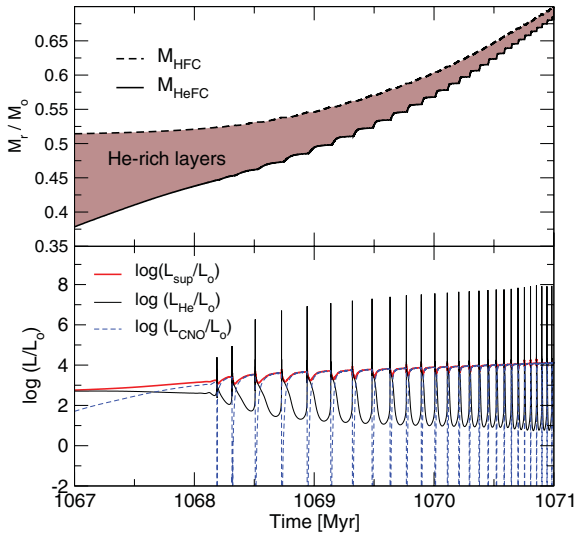

Figure 2. Upper panel: change in the He content in the region limited by the boundaries of the HeFC and the HFC during the thermally pulsing AGB phase. Lower panel: the temporal evolution of surface luminosity and H- and He-burning luminosities in solar units for our initially 2 $M_\odot$ star during the thermally pulsing AGB phase.

reduction is due mainly to the increase of the mass of the future white dwarf, that grows from $M_{\rm fWD} = 0.523$ to $0.7114\,M_\odot$ between the thermal pulses 1 and 30.

Our experiment shows that the He mass left in a DA white dwarf could be as much as a *factor* of 3–4 lower than the values predicted by standard evolutionary computations, but not 2 or 3 *orders of magnitude* lower, which would be necessary for g-mode periods to be substantially affected. We conclude that we can safety ignore the variation of $M_{\rm He}$ in our asteroseismological analysis of ZZ Ceti stars.

2.3 The model grid

The DA white dwarf models employed in this study are the result of full evolutionary calculations of progenitor stars for solar-like metallicity ($Z = 0.01$). The complete evolution of eleven evolutionary sequences with initial stellar mass in the range 1–5 $M_\odot$ has been computed from the ZAMS through the thermally pulsing and mass-loss phases on the AGB and finally to the domain of planetary nebulae. The values of the stellar mass of our set of models are shown in the upper row of Table 1. The range of stellar mass covered by our computations comfortably accounts for the stellar mass of most of the observed pulsating DA white dwarfs.

Our asteroseismological approach basically consists in the employment of detailed white dwarf models characterized by very accurate physical ingredients. These models are obtained by computing the complete evolution of the progenitor stars. We have applied successfully this approach to the hot DOVs or GW Vir stars (see Córsico et al. 2007a,b, 2008, 2009). Since the final chemical stratification of white dwarfs is fixed in prior stages of their evolution, the evolutionary history of progenitor stars is of utmost importance in the context of white dwarf asteroseismology. Our asteroseismological approach, while being physically sounding, is by far much more computationally demanding than other approaches in which simplified models are used. As a result, our approach severely limits the exploration of the parameter space of the models. Indeed, for the case of DA white dwarfs, we have only two parameters which we are able to vary in a consistent way: the stellar mass (M_*) and the effective temperature ($T_{\rm eff}$). Instead, the thickness of the H envelope ($M_{\rm H}$), the content of He ($M_{\rm He}$), the shape of the C–O chemical structure at the core (including the precise proportions of central O and C), and the thickness of the chemical transition regions are fixed by the evolutionary history of progenitor stars. Therefore, to push on the limits of our asteroseismological exploration, it would be desirable to change some additional parameters besides the stellar mass and effective temperature of our DA models. In this work, we have chosen to vary the thickness of the H envelope, because of the uncertainties in the mass-loss rates. According to full evolutionary computations (Althaus et al. 2010b), the maximum H envelope mass expected in a white dwarf depends on the stellar mass and ranges from $M_{\rm H}/M_* \sim 2.4 \times 10^{-4}$ (for $M_* = 0.525 M_\odot$) to 8.5×10^{-6} (for $M_* = 0.878 M_\odot$) (see the first row of Table 1). Our decision for changing this parameter is due to several reasons: first, there are compelling theoretical reasons to believe that the H content of DA white dwarfs might depend on the details of their previous evolution. On the contrary, the He content or the inner C–O chemical profiles are not expected to vary significantly due to the details of the previous evolutionary history (with the exception of a possible merger origin for the white dwarfs). Indeed, the total H content remaining in some DA white dwarfs could be several orders of magnitude lower than that predicted by our standard treatment of progenitor evolution. For instance, Althaus et al. (2005) have found that $M_{\rm H}$ becomes considerably reduced if the progenitor experiences a late thermal pulse episode (LTP) shortly after the departure from the thermally pulsing AGB phase. In this sense, Tremblay & Bergeron (2008) show that the increase in the ratio of He- to H-rich white dwarfs can be understood on the basis that a fraction of DA white dwarfs above $T_{\rm eff} \approx 10\,000$ K are characterized by a broad range of H-layer thickness. Second, the precise location of the He/H transition region (and the value of $M_{\rm H}$) strongly affects the structure of the adiabatic period spectrum in a DA white dwarf (Bradley 1996). Finally, $M_{\rm H}$ is the structural parameter that can be more easily modified in our models without removing relevant features predicted by the complete progenitor evolution.

In order to get different thicknesses of the H envelope, we have followed a simple recipe. For each sequence characterized by a given stellar mass and a thick value of $M_{\rm H}$, as predicted by the full computation of the pre-white dwarf evolution (second row of Table 1), we have simply replaced ^{1}H by ^{4}He at the basis of the H envelope. This is done at very high effective temperatures ($\gtrsim 70\,000$ K), in such a way that the unphysical transitory effects associated to this procedure end much long before the models reach the stage of pulsating DA white dwarfs. After our ad hoc procedure to change the thickness of the H envelope, we allow time-dependent element diffusion to operate while the models cool down until they reach the effective temperatures characterizing the DAV instability strip. Diffusion leads to very smooth chemical profiles at the He/H chemical transition regions. The resulting values of the H content for the different envelopes are shown in Table 1, and a graphical representation of the basic grid of models employed in this work is displayed in Fig. 1. In this figure, the canonical values of $M_{\rm H}$ predicted by stellar evolution are connected with a thick (orange) line. Obviously, beyond the availability of the models of this coarse grid, we have the capability to generate additional DA white dwarf evolutionary sequences with arbitrary values of $M_{\rm H}$ for each stellar mass in order to refine the model grid.

Table 1. The values of the stellar mass of our set of DA white dwarf models (upper row) and the mass of H corresponding to the different envelope thicknesses considered for each stellar mass. The second row shows the maximum value of the thickness of the H envelope for each stellar mass according to our evolutionary computations.

$M_*/M_\odot$	0.5249	0.5480	0.5701	0.5932	0.6096	0.6323	0.6598	0.7051	0.7670	0.8373	0.8779
$\log(M_H/M_*)$	−3.62	−3.74	−3.82	−3.93	−4.02	−4.12	−4.25	−4.45	−4.70	−5.00	−5.07
	−4.27	−4.27	−4.28	−4.28	−4.45	−4.46	−4.59	−4.88	−4.91	−5.41	−5.40
	−4.85	−4.85	−4.84	−4.85	−4.85	−4.86	−4.87	−5.36	−5.37	−6.36	−6.39
	−5.35	−5.35	−5.34	−5.34	−5.35	−5.35	−5.35	−6.35	−6.35	−7.36	−7.38
	−6.33	−6.35	−6.33	−6.33	−6.34	−6.34	−6.35	−7.35	−7.34	−8.34	−8.37
	−7.34	−7.33	−7.34	−7.34	−7.33	−7.35	−7.33	−8.34	−8.33	−9.34	−9.29
	−8.33	−8.33	−8.31	−8.33	−8.33	−8.33	−8.33	−9.34	−9.33	–	–
	−9.25	−9.22	−9.33	−9.33	−9.25	−9.34	−9.33	–	–	–	–

2.4 Pulsation computations

We carried out the adiabatic pulsation computations required by the present asteroseismological analysis by employing the non-radial pulsation code described in Córsico & Althaus (2006). Briefly, the code, which is coupled to the LPCODE evolutionary code, is based on the general Newton–Raphson technique and solves the full fourth-order set of equations governing linear, adiabatic, non-radial stellar pulsations following the dimensionless formulation of Dziembowski (1971). The prescription used to assess the run of the Brunt–Väisälä frequency (N) is the so-called 'Ledoux modified' treatment (see Tassoul et al. 1990) appropriately generalized to include the effects of having three nuclear species varying in abundance.

In the lower panel of Fig. 3 we show the spatial run of the logarithm of the squared Brunt–Väisälä frequency for models with $M_* = 0.609\,M_\odot$ and different values of the thickness of the H envelope for $T_{\rm eff} \approx 12\,000$ K. In the upper panel, we plot the internal chemical stratification of the models for the main nuclear species. The figure emphasizes the role of the chemical interfaces on the shape of the Brunt–Väisälä frequency. In fact, each chemical transition region produces clear and distinctive features in N, which are eventually responsible for the mode-trapping properties of the models. In the core region, there are several peaks at $-\log(q) \approx 0.4$–0.5 (where

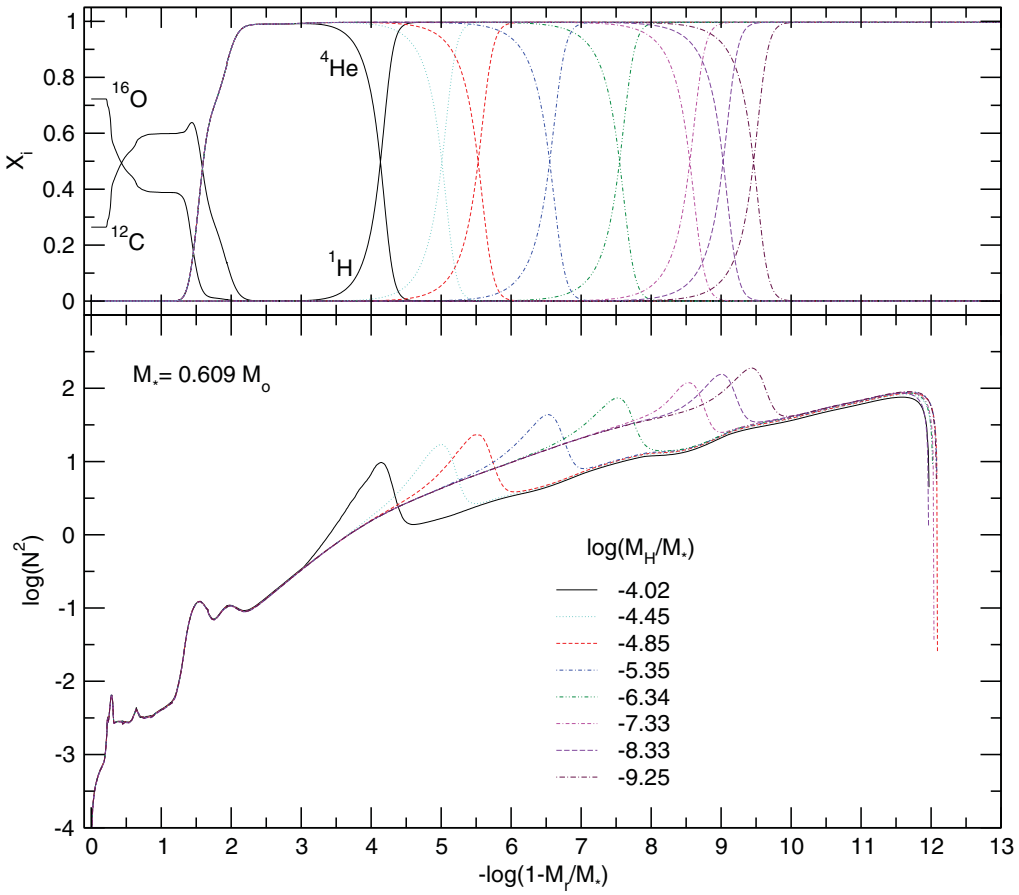

Figure 3. Upper panel: the internal chemical profiles of DA white dwarf models with $M_* = 0.609\,M_\odot$, $T_{\rm eff} \sim 12\,000$ K and different thicknesses of the H envelope. Only the main nuclear species are depicted. Lower panel: the run of the logarithm of the squared Brunt–Väisälä frequency for each model. Note the correspondence between the chemical transition regions (upper panel) and the resulting features in the shape of the Brunt–Väisälä frequency. For details, see the text.

$q \equiv 1 - M_r/M_*$) resulting from steep variations in the inner C–O profile. The step shape of the C and O abundance distribution within the core, which is due to the occurrence of extra mixing episodes beyond the fully convective core during central helium burning, constitutes an important source of mode trapping in the core region – 'core-trapped' modes (see Córsico & Althaus 2006). The extended bump in N^2 at $-\log(q) \approx 1$–2 is another relevant source of mode trapping. This feature is caused by the chemical transition of He, C and O resulting from nuclear processing in prior AGB and thermally pulsing AGB stages. It is worth noting that the shape of this transition is affected by diffusion processes which are operative at these evolutionary stages. Finally, there is the He/H transition region, which is also another source of mode trapping, in this case associated with modes trapped in the outer H envelope.

We have performed pulsation calculations on about $(11 \times 7 \times 200) = 15\,400$ DA white dwarf models. In this account, we have considered the number of stellar mass values (11), the number of thicknesses of the H envelope for each sequence ($\approx$7), and the number of models ($\approx$200) with effective temperature in the interval 14 000–9000 K, respectively. For each model, adiabatic pulsation g-modes with $\ell = 1$ and 2 and periods in the range 80–2000 s have been computed. This range of periods corresponds (on average) to $1 \lesssim k \lesssim 50$ for $\ell = 1$ and $1 \lesssim k \lesssim 90$ for $\ell = 2$. So, more than $\sim 2 \times 10^6$ adiabatic pulsation periods have been computed in this work.

3 ASTEROSEISMOLOGICAL FITS

We search for an asteroseismological model that best matches the pulsation periods of our target stars. To this end, we seek the model that minimizes a quality function defined simply as the average of the absolute differences between theoretical and observed periods (e.g. Bradley 1998):

$$\Phi = \Phi(M_*, M_{\rm H}, T_{\rm eff}) = \frac{1}{N} \sum_{i=1}^{N} |\Pi_k^{\rm th} - \Pi_i^{\rm obs}|, \quad (1)$$

where N is the number of the observed periods in the star under study. We also have considered the quality function defined as (e.g. Córsico et al. 2009)

$$\chi^2 = \chi^2(M_*, M_{\rm H}, T_{\rm eff}) = \frac{1}{N} \sum_{i=1}^{N} \min \left[\Pi_k^{\rm th} - \Pi_i^{\rm obs}\right]^2. \quad (2)$$

Finally, we employ the following merit function (e.g. Castanheira & Kepler 2008):

$$\Xi = \Xi(M_*, M_{\rm H}, T_{\rm eff}) = \sum_{i=1}^{N} \sqrt{\frac{\left[\Pi_k^{\rm th} - \Pi_i^{\rm obs}\right]^2 A_i}{\sum_{i=1}^{N} A_i}}, \quad (3)$$

where the amplitudes A_i are used as weights of each observed period. In this way, the period fit is more influenced by modes with large amplitudes than by the ones with low amplitudes.

In the asteroseismological analysis of this work, we have employed the three quality functions Φ, χ^2 and Ξ, defined by equations (1), (2) and (3), respectively. Since generally these functions lead to very similar results, we shall describe the quality of our period fits in terms of the function $\Phi = \Phi(M_*, M_{\rm H}, T_{\rm eff})$ only. The effective temperature, the stellar mass and the mass of the H envelope of our DA white dwarf models are allowed to vary in the ranges $14\,000 \gtrsim T_{\rm eff} \gtrsim 9000$ K, $0.525 \lesssim M_* \lesssim 0.877\,{\rm M}_\odot$, $-9.4 \lesssim \log(M_{\rm H}/M_*) \lesssim -3.6$, where the ranges of the values of $M_{\rm H}$ are dependent on M_* (see Table 1 and Fig. 1). For simplicity, the mass of He has been kept fixed at the value predicted by the evolutionary computations for each sequence. As we discussed in Section 2.2, the mass of the He content is not expected to be substantially smaller (say 100–1000 times) than predicted by our modelling. For this not too large uncertainty in the He content, only a weak dependence of the g-mode adiabatic pulsation periods on the value of $M_{\rm He}$ is expected (Bradley 1996), at variance with what happens with $M_{\rm H}$. Finally, artificially changing the He mass of our models would imply moving the triple transition C–O/He, which should introduce serious and undesirable artificial changes in the chemical structure of the models. The shape of the C–O chemical profile at the core and the central abundances of O and C have been also kept fixed according the predictions of the evolution during the central He burning stage of the progenitors. Finally, the thicknesses of the C–O/He and the He/H chemical transition regions have also been kept fixed at the values dictated by time-dependent element diffusion.

4 STARS ANALYSED AND RESULTS

We have carried out asteroseismological fits for a set of 44 bright ZZ Ceti stars, the atmospheric parameters of which are shown in columns 2 and 3 of Table 2. In this table, the stars have been sorted by decreasing $T_{\rm eff}$. The location of the studied stars in the $\log g$–$T_{\rm eff}$ plane is displayed in Fig. 4 along with our evolutionary tracks. We defer to a future work the study of the fainter ZZ Ceti stars discovered within the SDSS. Most of these stars have been included in the study of Castanheira & Kepler (2009).

In this section we present the results of our asteroseismological inferences. Because G117−B15A is the benchmark of the ZZ Ceti class, we will devote the complete Section 4.2 to describe in detail the results of our asteroseismological analysis for this star, including a discussion of our findings, and defer the presentation of results for the whole sample of the analysed stars to the subsequent section. Before going to the description of our asteroseismological results, we briefly examine below the spectroscopic masses derived for the studied DAV stars and how the average value fits to the mean mass of DA white dwarfs reported by recent works.

4.1 Spectroscopic masses

The spectroscopic masses of the 44 ZZ Ceti stars studied in this work are shown in column 4 of Table 2. They have been derived simply interpolating from the tracks in the $\log g$–$T_{\rm eff}$ diagram given the values of $\log g$ and $T_{\rm eff}$ inferred from spectroscopic analysis. The mean value of the spectroscopic masses for our sample of DAV stars is $\langle M_* \rangle_{\rm spec} = 0.630 \pm 0.028\,{\rm M}_\odot$. It is interesting to compare this value with the average mass of DA (pulsating and not pulsating) white dwarfs according to recent studies. Our value is somewhat higher ($\sim$4 per cent) than the value reported by Kepler et al. (2010) for DA white dwarfs on the basis of a large sample of 1505 stars of the SDSS (DR4), $\langle M_* \rangle_{\rm DA} = 0.604 \pm 0.003\,{\rm M}_\odot$, and in agreement with the recent determination of Falcon et al. (2010), $\langle M_* \rangle_{\rm DA} = 0.647^{+0.013}_{-0.014}\,{\rm M}_\odot$, obtained from the gravitational redshift determination of 449 DA white dwarfs, and that of Tremblay, Bergeron & Gianninas (2011), $\langle M_* \rangle_{\rm DA} = 0.613\,{\rm M}_\odot$, using 1089 DAs from DR4 of the SDSS.

4.2 The archetypal ZZ Ceti star G117−B15A

For this star, we initially computed the merit functions through our model grid by assuming that the harmonic degree of the three observed periods of G117−B15A is $\ell = 1$ from the outset. Somewhat disappointing, we did not find any stellar model of the basic grid that matched simultaneously the three observed periods. By closely examining our results, we discovered that a good period fit could be

Table 2. Atmospheric parameters and spectroscopic masses for the sample of ZZ Ceti stars analysed in this paper.

Star	$T_{\rm eff}$ (K)	$\log g$	$M_*/{\rm M}_\odot$	Ref.
G226−29	12 460 ± 200	8.28 ± 0.05	0.771 ± 0.032	3
HS 1531+7436	12 350 ± 181	8.17 ± 0.048	0.704 ± 0.029	1
G185−32	12 130 ± 200	8.05 ± 0.05	0.634 ± 0.028	3
L19−2	12 100 ± 200	8.21 ± 0.05	0.726 ± 0.033	3
G132−12	12 080 ± 200	7.94 ± 0.05	0.575 ± 0.026	4
EC 11507−1519	12 030 ± 200	7.98 ± 0.05	0.596 ± 0.026	4
PG 1541+650	12 000 ± 70	7.79 ± 0.04	0.502 ± 0.023*	6
R548	11 990 ± 200	7.97 ± 0.05	0.590 ± 0.026	3
GD 165	11 980 ± 200	8.06 ± 0.05	0.639 ± 0.029	3
GD 66	11 980 ± 200	8.05 ± 0.05	0.634 ± 0.028	3
G207−9	11 950 ± 200	8.35 ± 0.05	0.812 ± 0.033	3
EC 14012−1446	11 900 ± 200	8.16 ± 0.05	0.696 ± 0.031	3
KUV 11370+4222	11 890 ± 200	8.06 ± 0.05	0.639 ± 0.028	3
G238−53	11 890 ± 200	7.91 ± 0.05	0.559 ± 0.025	3
GD 99	11 820 ± 200	8.08 ± 0.05	0.650 ± 0.028	3
G29−38	11 820 ± 200	8.14 ± 0.05	0.684 ± 0.030	3
LP 133−144	11 800 ± 200	7.87 ± 0.05	0.539 ± 0.025	3
HS 1249+0426	11 770 ± 181	7.92 ± 0.048	0.564 ± 0.024	1
MCT 2148−2911	11 740 ± 200	7.82 ± 0.05	0.515 ± 0.023*	5
GD 385	11 710 ± 200	8.04 ± 0.05	0.627 ± 0.028	3
GD 244	11 680 ± 200	8.08 ± 0.05	0.650 ± 0.028	2
HS 0507+0434B	11 630 ± 200	8.17 ± 0.05	0.702 ± 0.030	3
G117−B15A	11 630 ± 200	7.97 ± 0.05	0.589 ± 0.026	3
EC 23487−2424	11 520 ± 200	8.10 ± 0.05	0.661 ± 0.028	3
MCT 0145−2211	11 500 ± 200	8.14 ± 0.05	0.684 ± 0.030	3
KUV 08368+4026	11 490 ± 200	8.05 ± 0.05	0.633 ± 0.028	3
PG 2303+243	11 480 ± 200	8.09 ± 0.05	0.655 ± 0.028	3
BPM 31594	11 450 ± 200	8.11 ± 0.05	0.666 ± 0.029	3
HLTau−76	11 450 ± 200	7.89 ± 0.05	0.548 ± 0.025	3
G255−2	11 440 ± 200	8.17 ± 0.05	0.702 ± 0.030	3
HE 1429−037	11 434 ± 36	7.82 ± 0.02	0.514 ± 0.010*	7
G191−16	11 420 ± 200	8.05 ± 0.05	0.632 ± 0.028	3
HE 1258+0123	11 400 ± 200	8.04 ± 0.05	0.627 ± 0.029	3
G232−38	11 350 ± 200	8.01 ± 0.05	0.610 ± 0.027	4
KUV 02464+3239	11 290 ± 200	8.08 ± 0.05	0.648 ± 0.028	2
HS 1625+1231	11 270 ± 181	8.06 ± 0.048	0.638 ± 0.027	1
BPM 30551	11 260 ± 200	8.23 ± 0.05	0.737 ± 0.032	3
HS 1824−6000	11 192 ± 181	7.65 ± 0.048	0.427 ± 0.030*	1
G38−29	11 180 ± 200	7.91 ± 0.05	0.557 ± 0.025	3
GD 154	11 180 ± 200	8.15 ± 0.05	0.689 ± 0.029	3
R808	11 160 ± 200	8.04 ± 0.05	0.626 ± 0.028	3
BPM 24754	11 070 ± 200	8.03 ± 0.05	0.620 ± 0.028	3
G30−20	11 070 ± 200	7.95 ± 0.05	0.578 ± 0.026	3
PG 1149+058	10 980 ± 181	8.10 ± 0.048	0.660 ± 0.027	1

References: 1 – Voss et al. (2006); 2 – Fontaine et al. (2003); 3 – Bergeron et al. (2004); 4 – Gianninas, Bergeron & Fontaine (2006); 5 – Gianninas, Bergeron & Fontaine (2005); 6 – Homeier et al. (1998); 7 – Silvotti et al. (2005).

Note. The values of the stellar mass marked with ∗ have been derived by extrapolation from our evolutionary model grid, and so, they are uncertain.

found by considering additional values of $M_{\rm H}$ near $10^{-6}M_*$ in the sequence with $M_* = 0.593\,{\rm M}_\odot$ at approximately $T_{\rm eff} = 12\,000$ K. Hence, we computed several additional sequences with different values of $M_{\rm H}$ until a best-fitting model with $\log(M_{\rm H}/M_*) = -5.903$ was found. The characteristics and periods of the best-fitting model are shown in row 1 (model 1) of Table 3. The period at 215 s has a radial order $k = 2$. Note that the fit to the main period is excellent ($|\Delta| \equiv |\Pi^{\rm obs} - \Pi^{\rm th}| = 0.015$ s), although the fits to the remainder two periods are not as good. The global fit, characterized by $\Phi = 1.729$ s, is still very satisfactory. We repeated our computations but assuming $\ell = 1$ for the 215 s mode at the outset, and allowing the other two periods to be associated with $\ell = 1$ or 2. We arrived at the same asteroseismological solution.

In Fig. 5 we plot the function $\Phi(M_*, M_{\rm H}, T_{\rm eff})$ in terms of the effective temperature for the different H envelope thicknesses corresponding to the sequence with $M_* = 0.593\,{\rm M}_\odot$. Clearly notorious is the existence of the best-fitting solution at $T_{\rm eff} \sim 12\,000$ K and $M_{\rm H}/M_* \approx 1.25 \times 10^{-6}$. Apart from the best-fitting solution, there is another minimum at $T_{\rm eff} \sim 10\,380$ K and $M_{\rm H}/M_* \approx 1.17 \times 10^{-4}$, where $\Phi \approx 4.5$ s. However, this solution must be discarded because its effective temperature is too low as compared with the limits imposed by spectroscopy for G117−B15A.

The uniqueness of the solution regarding the thickness of the H envelope is one of the main results of this work for G117−B15A. However, we warn that in this study we are matching three observed quantities (the pulsation periods of G117−B15A) by varying just three structural quantities (M_*, $M_{\rm H}$, and $T_{\rm eff}$). So, it is not unconceivable that if we were varying an additional parameter (for instance $X_{\rm O}$, $M_{\rm He}$, etc.) of our models, we could found multiple asteroseismological solutions due to the ambiguity introduced by the new parameter to be adjusted. Our models do not have an extra fit parameter.

We also carried out additional period fits in which the value of ℓ for each of the theoretical periods is not fixed but instead is obtained as an output of our period fit procedure, although the allowed values are just $\ell = 1$ and 2. The results are displayed in rows 2–4 of Table 3. For these models, the period fits are excellent. In particular, the periods of model 2 match the observed periods with an average difference of ∼0.18 s. One of the reasons is that are more $\ell = 2$ modes per period interval. However, for the three models, the main periodicity of G117−B15A at 215 s is associated to a $\ell = 2$ mode. This is in strong contradiction with the results of Robinson et al. (1995), who identify the 215 s period with a $\ell = 1$ mode by means of time-resolved UV spectroscopy. This result is consistent with the further analysis of Kotak, van Kerkwijk & Clemens (2004). Thus, as tempting as these solutions seem, they must all be discarded from our analysis.

4.2.1 *Estimation of the internal uncertainties*

We have assessed the uncertainties in the stellar mass (σ_{M_*}), the thickness of the H envelope ($\sigma_{M_{\rm H}}$) and the effective temperature ($\sigma_{T_{\rm eff}}$) of the best-fitting model by employing the expression (Zhang, Robinson & Nather 1986; Castanheira & Kepler 2008)

$$\sigma_i^2 = \frac{d_i^2}{(S - S_0)}, \tag{4}$$

where $S_0 \equiv \Phi(M_*^0, M_{\rm H}^0, T_{\rm eff}^0)$ is the minimum of Φ which is reached at $(M_*^0, M_{\rm H}^0, T_{\rm eff}^0)$ corresponding to the best-fitting model, and S is the value of Φ when we change the parameter i (in this case, M_*, $M_{\rm H}$ or $T_{\rm eff}$) by an amount d_i, keeping fixed the other parameters. The quantity d_i can be evaluated as the minimum step in the grid of the parameter i. We obtain the following uncertainties, which are the *internal* errors of our asteroseismic procedure: $\sigma_{M_*} \sim 0.007\,{\rm M}_\odot$, $\sigma_{M_{\rm H}} \sim 0.7 \times 10^{-6}M_*$ and $\sigma_{T_{\rm eff}} \sim 200$ K. The uncertainties in the other quantities (L_*, R_*, g, etc.) are derived from the uncertainties in M_* and $T_{\rm eff}$.

In Table 4, we compare the main characteristics of our best-fitting model with the observed properties of G117−B15A. In particular, we include the surface parameters of G117−B15A taken from several spectroscopic studies. We include also the spectroscopic mass computed by interpolating from our evolutionary tracks. Note the

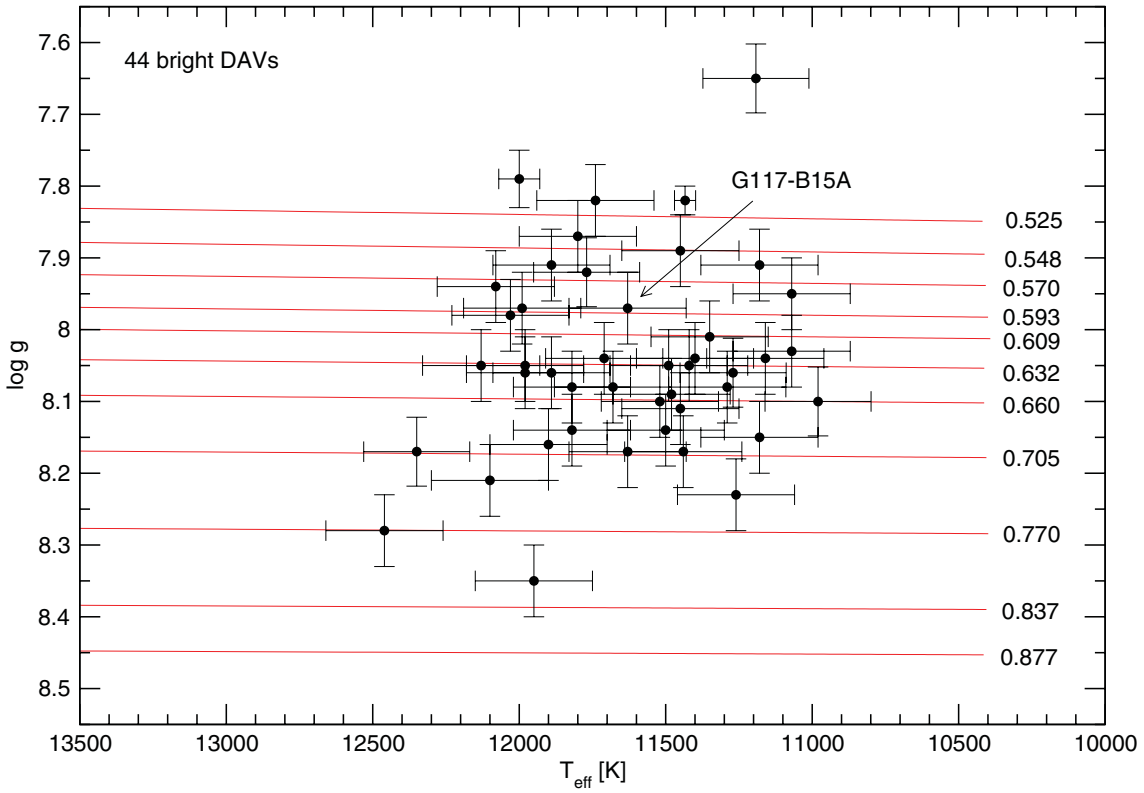

Figure 4. The location of the 44 ZZ Ceti stars analysed in this paper in the $\log g$–$T_{\rm eff}$ plane. The lines correspond to our set of DA white dwarf evolutionary tracks with thick (canonical) H envelope thickness.

Table 3. Possible asteroseismological solutions for G117−B15A. Model 1 is the best-fitting model corresponding to a family of solutions obtained by imposing that all of the observed periods correspond to $\ell = 1$ modes. Models 2–4 result from the assumption that the observed periods are associated to $\ell = 1$ or 2 modes.

Model	$T_{\rm eff}$ (K)	$M_*/{\rm M}_\odot$	$\log(M_{\rm He}/M_*)$	$\log(M_{\rm H}/M_*)$	$\Pi_i^{\rm obs}$ (s)	$\Pi_k^{\rm th}$ (s)	ℓ	k	$\lvert\Delta\rvert$ (s)	Φ (s)
1	11 986	0.5932	−1.62	−5.90	215.20	215.215	1	2	0.015	1.729
					270.46	273.437	1	3	2.977	
					304.05	301.854	1	4	2.196	
2	12 450	0.6090	−1.61	−4.45	215.20	214.947	2	6	0.253	0.177
					270.46	270.268	2	8	0.192	
					304.05	304.136	2	9	0.086	
3	12 219	0.6598	−1.91	−8.33	215.20	215.218	2	5	0.018	0.526
					270.46	270.406	1	3	0.054	
					304.05	305.557	2	8	1.507	
4	11 735	0.5930	−1.62	−9.33	215.20	214.422	2	4	0.778	0.735
					270.46	271.682	1	2	1.222	
					304.05	303.846	2	7	0.204	

agreement between the effective temperature and gravity of our asteroseismological model and the values derived by Koester & Allard (2000) and Koester & Holberg (2001). The total mass of our model, however, is 3–11 per cent higher than the values derived in those studies. Our model is ∼350 K hotter than the spectroscopic temperature of Bergeron et al. (1995a, 2004), and about 400 K cooler than the value derived by Robinson et al. (1995), but the surface gravity and mass are in excellent agreement with the values quoted in both studies.

4.2.2 *Asteroseismological distance*

Since we have the luminosity of the best-fitting model, we can estimate the asteroseismological distance and parallax of G117−B15A by means of the relation $\log d\,({\rm pc}) = (1/5)(m_{\rm V} - M_{\rm V} + 5)$, where $M_{\rm V} = M_{\rm bol} - BC$. The bolometric magnitude, $M_{\rm bol}$, can be computed as $M_{\rm bol} = {\rm M}_{\rm bol}(\odot) - 2.5\log(L_*/{\rm L}_\odot)$, being the bolometric magnitude of the Sun $M_{\rm bol}(\odot) = +4.75$ (Allen 1973). By using $BC = -0.611$ (Bergeron et al. 1995a) and $m_{\rm V} = 15.50$ (Bergeron

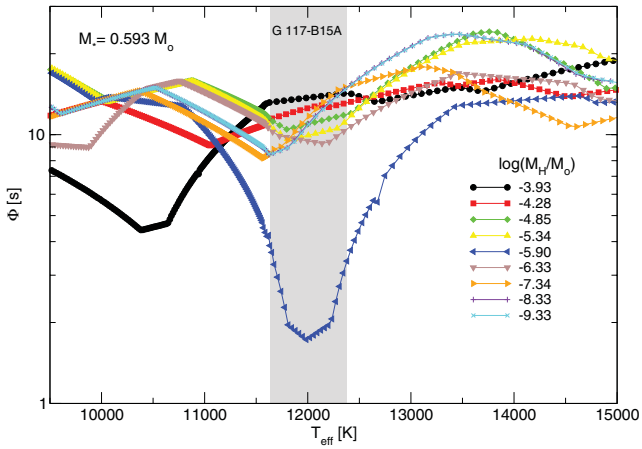

Figure 5. The quality function $\Phi(M_*, M_H, T_{eff})$ in terms of T_{eff} for the different values of the hydrogen thickness (shown with different colours and symbols) and a stellar mass of $M_* = 0.593\,M_\odot$. The grey strip corresponds to the effective temperature of G117−B15A according to spectroscopic analysis. Note in particular the location of the best-fitting solution (the minimum of Φ at $T_{eff} \sim 12\,000$ K), corresponding to the model 1 ($\ell = 1$, $k = 2, 3, 4$) in Table 3.

et al. 1995b), we obtain a distance $d = 60.3 \pm 2.5$ pc, and a parallax $\pi = 16.6 \pm 0.8$ mas, in excellent agreement with the inference of Bradley (1998) ($\pi = 16.5$ mas). The distance estimated from optical, *IUE* and *HST* spectra is 58 ± 2, 59 ± 5 and 67 ± 9 pc, respectively. Holberg, Bergeron & Gianninas (2008) derive a distance of 57.68 ± 0.60 pc. Our seismological parallax is larger than the trigonometric value extracted from the Yale Parallax Catalog (van Altena, Lee & Hoffleit 1994) of 10.5 ± 4.2 mas. In order for the asteroseismological parallax to be compatible with the trigonometric one, the mass of the asteroseismological model should be as low as ≈0.35 $M_\odot$! We can safely discard a low stellar mass for G117−B15A from spectroscopy. Then, we conclude that the trigonometric parallax must be more uncertain than quoted, and that the asteroseismological parallax is robust.

4.2.3 *Discussion*

All the previous asteroseismological studies on G117−B15A (Bradley 1998; Benvenuto et al. 2002; Bischoff-Kim et al. 2008a; Castanheira & Kepler 2008) report an ambiguity of the solutions regarding the thickness of the H envelope of this star. In those studies, a family of thin envelope solutions is obtained for a identification $k = 1, 2, 3$, whereas a second family of solutions of thick envelopes is derived if $k = 2, 3, 4$. In contrast, our asteroseismological analysis strongly points to a single solution regarding the thickness of the H envelope, with a value of $\log(M_H/M_*) \sim -5.9$, that corresponds to the identification $k = 2, 3, 4$, which was associated to thick H envelopes in the previous studies. The degeneracy of solutions is solved for the first time by our results. The reason for the uniqueness of the solution in our computations is that, regardless of the value of the stellar mass, temperature, or thickness of the H envelope, it is impossible to find a model whose mode with $k = 1$ has a period close to 215 s. This preclude us to find any possible asteroseismological model with the identification $k = 1, 2, 3$. This is shown in Fig. 6, where we plot the periods in terms of the thickness of the H envelope for models with $T_{eff} \sim 12\,000$ K and $M_* = 0.525\,M_\odot$ (left-hand panel), $M_* = 0.593\,M_\odot$ (middle panel) and $M_* = 0.877\,M_\odot$ (right-hand panel). In the middle panel, the best-fitting model is indicated with a dashed (brown) line. Clearly, the period for the mode with $k = 1$ in our models is always very short in comparison with the shortest period shown by G117−B15A. We mention that we have also computed an additional evolutionary sequence with the same characteristics as our best-fitting model, but with a thinner H envelope than that considered in Table 1 ($\log(M_H/M_*) < -9.33$). Even in this case, the pulsation periods exhibit the same trend shown in the middle panel Fig. 6, with the period of the $k = 1$ mode markedly departed from 215 s, and as a result, we are not able to find a thin-envelope solution.

It should be kept in mind, however, that we could run into multiple solutions for G117−B15A if we were to vary an additional parameter of our models. For instance, it could be possible that if we were freely changing the He content (M_{He}) of our models, for instance by adopting a He layer mass two order of magnitude thinner, then the $k = 1$ period could became close to 215 s, and so, we could recover the two families of thin and thick He envelope solutions found in the previous studies. However, as discussed in Section 2.2, such low M_{He} values are difficult to conceive from stellar evolution calculations.

A distinctive feature shown in Fig. 6 is the presence of a behaviour reminiscent to the well known 'avoided crossing' (see also fig. 3 of Castanheira & Kepler 2008). When a pair of modes experiences avoided crossing, the modes exchange their intrinsic properties (see

Table 4. Characteristics of G117−B15A and of our seismological model. The quoted uncertainties in the seismological model are the internal errors of our period-fit procedure. The progenitor star of the asteroseismological model star has a stellar mass of $M_* = 1.75\,M_\odot$ at the ZAMS.

Quantity	Robinson et al. (1995)	Koester & Allard (2000)	Koester & Holberg (2001)	Bergeron et al. (1995a, 2004)	Our seismological model
T_{eff} (K)	12 375 ± 125	11 900 ± 140	12 010 ± 180	11 630 ± 200	11 985 ± 200
$M_*/M_\odot$	0.591 ± 0.031	0.534 ± 0.072	0.575 ± 0.092	0.589 ± 0.026	0.593 ± 0.007
$\log g$	7.97 ± 0.06	7.86 ± 0.14	7.94 ± 0.17	7.97 ± 0.05	8.00 ± 0.09
$\log(R_*/R_\odot)$	–	–	–	–	−1.882 ± 0.029
$\log(L_*/L_\odot)$	–	–	–	–	−2.497 ± 0.030
M_{He}/M_*	–	–	–	–	2.39×10^{-2}
M_H/M_*	–	–	–	–	$(1.25 \pm 0.7) \times 10^{-6}$
X_C, X_O (centre)	–	–	–	–	0.28, 0.70

Note 1. The values of the spectroscopic mass quoted in columns 2–5 have been computed by interpolating from our set of evolutionary tracks (see Fig. 4) using the corresponding values of $\log g$ and T_{eff}.
Note 2. Robinson et al. (1995) use MLT/$\alpha = 1$ model atmospheres, while the other use MLT/$\alpha = 0.6$, hence they obtain lower T_{eff}s.

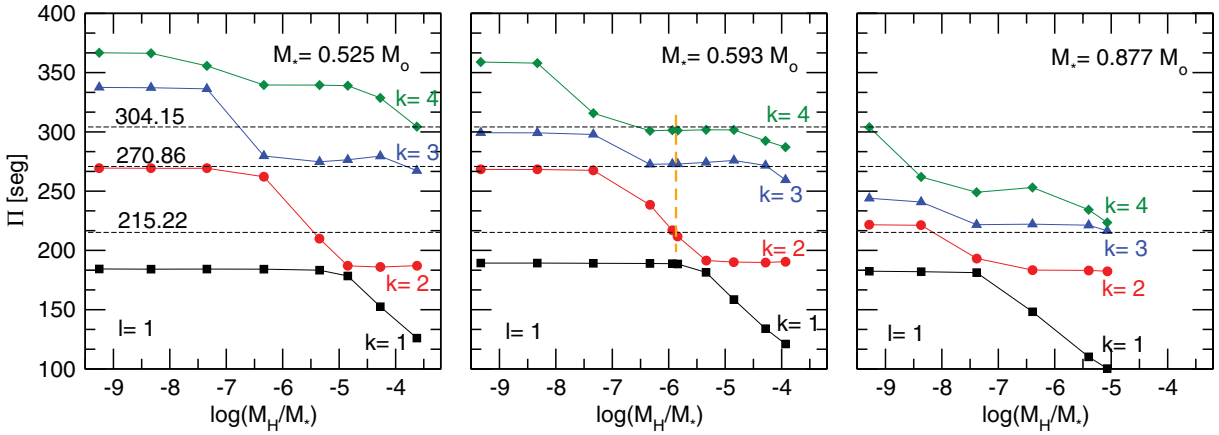

Figure 6. The periods of the modes with $\ell = 1$ and $k = 1$, 2, 3 and 4 in terms of the thickness of the H envelope corresponding to $M_* = 0.525\,M_\odot$ (left-hand panel), $M_* = 0.593\,M_\odot$ (middle panel) and $M_* = 0.877\,M_\odot$ (right-hand panel). The observed periods of G117−B15A are shown with thin horizontal dashed lines. The dashed (orange) line in the middle panel indicates the match between the theoretical periods of the asteroseismological model and the periods observed in G117−B15A.

Aizenman, Smeyers & Weigert 1977). In our models, avoided crossing is produced when we vary the thickness of the H envelope. As a result, for certain values of M_H, the period spacing turns out be very short. This effect is more notorious for low radial order modes. For instance, for the sequence with $M_* = 0.525\,M_\odot$, the period spacing between the modes with $k = 1$ and 2 is of only $\approx$8 s if $\log(M_H/M_*) \sim -4.8$! Something similar is seen for the sequences with $M_* = 0.593\,M_\odot$ and $M_* = 0.877\,M_\odot$, with H envelopes of $\log(M_H/M_*) \sim -5.3$ and $\log(M_H/M_*) \sim -7.4$, respectively. We note also that avoided crossing is present in our models, but to a less extent, when we vary the effective temperature.

In Figs 7 and 8, we display the thin and thick envelope solutions with empty and filled symbols, respectively, for the asteroseismological solutions found in previous works. The location of our asteroseismological model is depicted with a (magenta) star symbol. Note that Bischoff-Kim et al. (2008a) found several equally valid asteroseismological models with thin and thick H envelopes for G117−B15A. Fig. 7 shows a clear correlation between the mass and the effective temperature of the solutions in the studies of Bradley (1998), Bischoff-Kim et al. (2008a) and Castanheira & Kepler (2008): cooler solutions have larger masses. The opposite trend is exhibited by the two solutions of Benvenuto et al. (2002). All the solutions of Bischoff-Kim et al. (2008a) and two solutions of Castanheira & Kepler (2008) are substantially more massive than the best-fitting models of Bradley (1998), Benvenuto et al. (2002) and our own asteroseismological model, and also than the estimations of the stellar mass of G117−B15A from spectroscopic studies.

The existence of two separate families of solutions regarding the thickness of the H envelope, as predicted by previous studies, is clearly emphasized in Fig. 8. Here, it is notable a correlation between M_H and M_*, according to which the more massive asteroseismological models have thinner envelopes. Curiously, this trend is in line with the predictions of the canonical evolutionary computations (Althaus et al. 2010b), which are shown with a thick (orange) line that connects the maximum values of M_H for different stellar masses. The figure also shows a notable agreement between the thin and thick solutions of Bradley (1998), Benvenuto et al. (2002) and Castanheira & Kepler (2008). In contrast, the solutions of Bischoff-Kim et al. (2008a) (both thin and thick) appear shifted toward smaller values of the H envelope thickness. In this

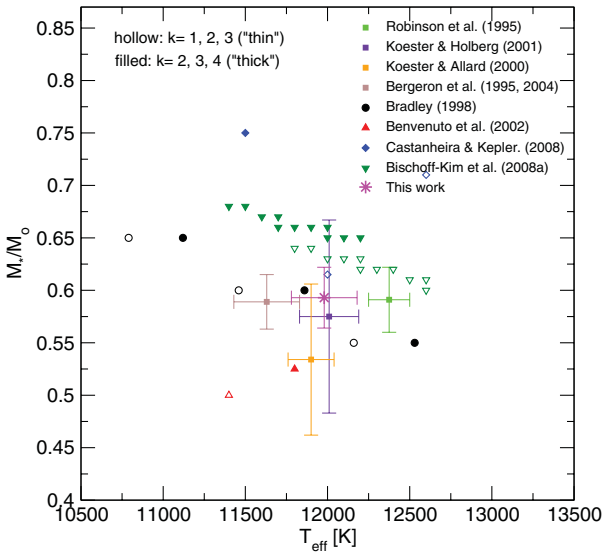

Figure 7. The location of the asteroseismological models for G117−B15A in the plane $T_{\rm eff}$–M_* according to the studies carried out up to date and according to this work, as indicated with different symbols. Empty symbols correspond to solutions for which the radial order identification of the observed periods is $k = 1$, 2, 3 (thin H envelopes), and filled symbols are associated to solutions for which the observed periods have $k = 2$, 3, 4 (thick H envelopes). Also included is the location of G117−B15A according to several spectroscopic studies (filled squares). Note that Robinson et al. (1995) use MLT/$\alpha = 1$ model atmospheres, while the other use MLT/$\alpha = 0.6$, hence they obtain lower $T_{\rm eff}$ values.

context, our single seismological solution seems to be more nearly compatible with the family of thin H envelopes (although with a mode identification typical of thick-envelope solutions) than with the group of thick envelopes.

Although our new value for the H envelope thickness of G117−B15A is significantly lower than the canonical value predicted by stellar evolution (roughly two orders of magnitude thinner), it is in perfect agreement with what could be expected from the LTP scenario. In this scenario, also called AGB final thermal pulse (AFTP) scenario, a final helium shell flash is experienced by a star shortly after the departure from the AGB (Blöcker 2001). During

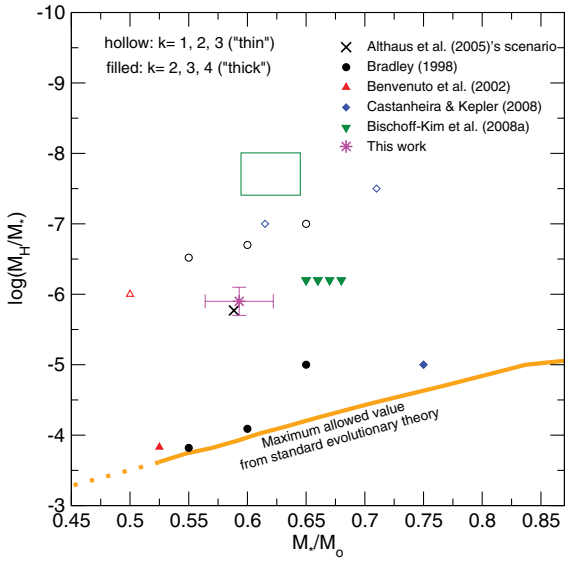

Figure 8. Similar to Fig. 7, but in the plane M_*–log (M_H/M_*). The hollow green rectangle corresponds to the thin solutions of Bischoff-Kim et al. (2008a) corresponding to an identification $k = 1, 2, 3$. In the interests of comparison, the location of the post-LTP remnant with a thin H envelope of the scenario of Althaus et al. (2005) is also shown.

a LTP, not all the hydrogen is burnt, in contrast to post-AGB stars that experience a very late thermal pulse (a born-again episode), but part is diluted by surface convection and mixed inwards with the underlying intershell region formerly enriched in helium, carbon and oxygen. Althaus et al. (2005) have explored the possibility that an initially 2.7 $M_\odot$ star experiencing a LTP shortly after the departure from the thermally pulsing AGB could reach the final cooling branch with a H envelope substantially smaller than predicted by standard stellar evolution. They found that most of the original H-rich material of the post-AGB remnant is burnt after the post-LTP evolution, when the star returns to the high $T_{\rm eff}$ regime for the second time, resulting in a white dwarf remnant of $M_* = 0.5885\,M_\odot$ with a value of the H envelope thickness of $M_H = 1.7 \times 10^{-6} M_*$. Very interestingly, our best-fitting model for G117−B15A and the DA white dwarf model resulting from the scenario proposed by Althaus et al. (2005) are located roughly at the *same* place in the plane M_*–log (M_H/M_*) (see Fig. 8).[1] Therefore, our study reinforces the validity of the results of Althaus et al. (2005) about the existence of DA white dwarfs with H envelopes substantially thinner than the canonical value, and suggests that G117−B15A could be the descendant of a progenitor star that experienced a LTP episode before reaching the final cooling branch.

4.3 The set of 44 ZZ Ceti stars

Here, we present the asteroseismological analysis for the 44 ZZ Ceti stars listed in Table 2, G117−B15A included. In the second and third columns of Table 5 we show the observed periods and amplitudes, respectively. These values are extracted from the works of Castanheira & Kepler (2008, 2009), unless indicated otherwise. The fourth

[1] We warn, however, that both models have different internal chemical structure, in particular due to the presence of extra chemical structure and appreciable amounts of ^{14}N at the base of the He buffer in the post-LTP DA white dwarf model of Althaus et al. (2005) (see the panel D of fig. 2 of Miller Bertolami, Alhaus & Córsico 2005).

Table 5. Periods observed in the sample of 44 bright ZZ Ceti stars studied in this work and the corresponding theoretical periods and (ℓ, k)-identification of our asteroseismological models.

Star	$\Pi^{\rm obs}$ (s)	A (mma)	$\Pi^{\rm th}$ (s)	ℓ	k	$\lvert\Delta\rvert$ (s)	Φ (s)
HS 1531+7436	112.50	···	112.499	1	1	0.001	0.001
GD 244[a]	202.98	4.04	195.973	2	5	7.007	2.165
	256.56	12.31	257.215	1	3	0.665	
	294.60	4.85	296.820	2	9	2.220	
	307.13	20.18	306.283	1	5	0.847	
	906.08	1.72	906.176	1	19	0.086	
G226−29	109.28	···	109.246	1	1	0.032	0.032
HS 0507+0434B	355.80	24.0	356.737	1	6	0.937	0.778
	446.20	13.9	446.429	1	8	0.229	
	555.30	16.6	556.767	1	11	1.468	
	743.40	7.6	742.920	1	16	0.679	
LP 133−144	209.20	10	211.247	1	2	2.047	1.256
	305.70	5.3	304.394	2	8	1.306	
	327.30	4.0	327.716	2	9	0.416	
EC 11507−1519	191.70	3.59	191.964	1	2	0.264	0.231
	249.60	7.70	249.798	1	4	0.198	
L19−2	113.80	2.4	113.313	2	2	0.487	1.224
	118.70	1.2	114.495	1	1	4.205	
	143.60	0.6	143.272	2	3	0.128	
	192.60	6.5	192.561	1	2	0.039	
	350.10	1.1	351.359	1	6	1.259	
GD 66[b]	197.65	4.21	198.104	2	4	0.450	0.871
	255.87	3.43	256.137	2	6	0.270	
	271.71	16.70	271.804	1	3	0.089	
	302.77	11.29	300.102	1	4	2.663	
G132−12	212.70	4.3	212.703	1	2	0.003	0.003
G207−9	259.10	17.3	258.853	1	4	0.247	0.767
	292.00	49.0	290.379	2	10	1.621	
	318.00	64.0	318.257	1	5	0.257	
	557.40	63.4	556.204	1	12	1.376	
	740.40	46.4	741.034	1	17	0.334	
G117−B15A	215.20	17.36	215.215	1	2	0.015	1.729
	270.46	6.14	273.437	1	3	2.977	
	304.05	7.48	301.854	1	4	2.196	
MCT 2148−2911	260.80	12.6	260.798	1	4	0.002	0.002
G38−29[c]	413.307	3.07	413.985	2	16	0.678	1.515
	432.354	3.57	434.227	2	17	1.873	
	546.960	6.97	545.442	2	22	1.519	
	705.970	18.44	707.049	1	16	1.079	
	840.390	5.19	839.307	1	20	1.083	
	899.971	10.59	896.903	2	38	3.068	
	922.567	5.94	921.066	2	39	1.591	
	945.448	12.34	946.328	2	40	0.880	
	962.007	8.09	962.277	1	23	0.270	
	963.593	4.58	962.277	1	23	1.316	
	989.719	10.04	993.0267	2	42	3.308	
	1002.16	7.14	1003.878	1	24	1.718	
	1016.15	5.79	1014.220	2	43	1.930	
	1081.82	5.04	1082.720	1	26	0.900	
PG 1541+650[d]	689.00	···	688.891	1	11	0.109	0.270
	757.00	···	757.047	1	12	0.047	
	564.00	···	563.346	2	16	0.654	
G191−16[h]	510.00	···	509.983	1	9	0.017	0.931
	600.00	···	598.812	1	11	1.188	

Table 5 – *continued*

Star	Π^{obs} (s)	A (mma)	Π^{th} (s)	ℓ	k	$\lvert\Delta\rvert$ (s)	Φ (s)
	710.00	···	712.027	1	14	2.027	
	893.00	···	893.495	1	18	0.495	
G185−32	215.74	1.93	215.739	1	2	0.001	1.691
	266.17	0.46	269.253	2	7	3.083	
	300.60	1.04	298.724	2	8	1.876	
	370.21	1.62	367.694	1	5	2.516	
	651.70	0.67	652.677	1	12	0.978	
EC 14012−1446	398.90	12.1	403.823	1	7	4.923	2.541
	530.10	16.7	524.782	1	10	5.318	
	610.40	54.3	613.677	1	12	3.277	
	678.60	7.6	675.620	1	14	2.980	
	722.90	22.9	721.733	1	15	1.167	
	769.10	51.7	769.121	1	16	0.042	
	882.70	2.9	883.878	2	34	1.178	
	937.20	11.0	934.485	2	36	2.715	
	1217.40	7.5	1216.141	1	27	1.259	
EC 23487−2424	804.50	19.3	806.160	1	19	1.660	2.297
	868.20	12.8	863.294	1	21	4.906	
	992.70	24.4	992.375	1	24	0.325	
GD 165	114.30	···	114.278	2	2	0.022	0.889
	120.36	···	119.195	1	1	0.445	
	192.68	···	192.102	1	2	0.578	
	249.90	···	252.412	1	3	2.512	
R548	187.28	0.9	187.597	1	1	0.308	2.516
	212.95	5.4	213.401	1	2	0.451	
	274.51	3.5	242.263	1	3	2.249	
	318.07	1.1	311.361	2	8	6.709	
	333.64	1.3	336.504	2	9	2.864	
HE 1258+0123	439.20	9.8	446.066	2	14	6.867	2.099
	528.50	9.3	527.704	1	9	0.796	
	628.00	15.2	627.326	2	21	0.679	
	744.60	22.9	744.780	1	14	0.180	
	881.50	17.6	892.728	1	17	1.228	
	1092.10	14.1	1094.947	1	22	2.847	
GD 154	402.60	0.3	404.998	1	5	2.398	0.903
	1088.60	2.0	1088.860	1	20	0.260	
	1186.50	2.4	1186.550	1	22	0.050	
GD 385	128.10	3.7	130.665	2	2	2.564	1.291
	256.00	11.2	255.983	1	3	0.017	
HE 1429−037	450.10	10.2	449.474	1	6	0.626	1.378
	826.40	18.3	829.489	1	14	3.089	
	969.00	12.7	968.924	1	17	0.076	
	1084.90	16.3	1080.279	1	19	4.621	
HS 1249+0426	288.90	7.55	288.905	1	4	0.005	0.005
G238−53	206.00	9.0	205.987	1	2	0.013	0.013
HS 1625+1231[e]	248.90	7.8	250.127	2	7	1.227	3.020
	268.20	13.3	274.612	1	3	6.412	
	325.50	13.3	320.910	1	5	4.590	
	353.00	10.7	351.912	2	11	1.088	
	385.20	17.0	382.670	1	6	2.530	
	425.80	13.9	461.967	1	7	6.167	
	533.60	23.6	531.504	1	9	2.096	
	862.90	48.9	862.949	1	17	0.049	
G29−38	218.70	1.5	217.321	2	4	1.379	2.841
	283.90	4.8	282.919	2	6	0.981	

Table 5 – *continued*

Star	Π^{obs} (s)	A (mma)	Π^{th} (s)	ℓ	k	$\lvert\Delta\rvert$ (s)	Φ (s)
	363.50	4.7	365.551	2	9	2.051	
	400.50	9.1	406.814	2	10	6.314	
	496.20	7.9	493.659	2	13	2.541	
	614.40	32.8	616.059	1	9	1.659	
	655.10	6.1	644.728	2	18	10.372	
	770.80	5.1	770.809	2	22	0.008	
	809.40	30.1	800.395	2	23	9.005	
	859.60	24.6	858.978	2	25	0.622	
	894.00	14.0	891.098	2	26	2.902	
	1150.50	3.6	1152.052	2	34	1.552	
	1185.60	3.4	1185.529	2	35	0.072	
	1239.90	1.9	1240.220	2	37	0.320	
PG 2303+243[f]	394.4	7.3	393.826	2	9	0.574	0.788
	616.4	31.4	616.560	1	8	0.160	
	863.8	7.4	862.711	2	24	1.089	
	965.3	19.7	966.590	1	15	1.290	
MCT 0145−2211	462.20	25	462.353	1	7	0.153	1.494
	727.90	19	726.912	1	13	0.988	
	823.20	15	826.663	1	15	3.463	
BPM 30551	606.80	11.5	607.055	1	12	0.255	0.175
	744.70	10.5	744.605	1	15	0.096	
GD 99	1311.00	5.0	1311.002	1	28	0.002	0.002
BPM 24754	643.70	···	643.330	2	21	0.370	0.938
	1045.10	···	1045.204	1	20	0.994	
	1234.10	···	1234.005	1	24	0.095	
	1356.60	···	1358.891	2	47	2.291	
KUV 02464+3239[g]	619.30	4.0	618.963	2	17	0.322	1.640
	777.60	5.5	779.541	1	12	1.931	
	829.70	11.6	829.913	2	24	1.229	
	866.20	9.5	860.447	2	25	5.704	
	993.20	13.2	992.707	1	16	0.717	
	1250.30	4.4	1250.374	1	21	0.121	
PG 1149+058	1023.50	10.5	1023.479	1	20	0.021	0.021
BPM 31594[h]	401.93	···	402.453	1	5	0.523	0.321
	617.28	···	617.162	1	10	0.118	
KUV 11370+4222	257.20	5.3	259.369	1	3	2.169	0.897
	292.20	2.5	291.687	1	4	0.513	
	462.90	3.2	462.919	2	15	0.019	
HS 1824−6000[e]	294.30	8.84	289.395	1	3	5.005	2.085
	304.40	7.66	301.198	2	8	3.202	
	329.60	13.56	329.587	1	4	0.013	
	384.40	3.30	384.520	2	11	0.120	
KUV 08368+4023	618.00	16.0	618.823	1	11	0.823	0.429
	494.50	5.5	494.464	2	16	0.036	
R808[c]	404.46	1.99	400.923	2	14	3.534	3.499
	511.27	4.49	514.497	1	10	3.231	
	632.18	3.41	629.270	2	24	2.909	
	745.12	3.97	747.750	1	16	2.630	
	796.25	3.97	799.402	2	31	3.149	
	842.71	2.81	844.484	2	33	1.777	
	860.23	3.48	865.257	2	34	5.030	
	875.15	3.73	870.376	1	19	4.770	
	911.53	3.19	913.952	1	20	2.418	
	915.80	5.54	615.230	2	36	0.573	
	952.39	3.36	945.909	1	21	6.483	

Table 5 – *continued*

Star	Π^{obs} (s)	A (mma)	Π^{th} (s)	ℓ	k	$\lvert\Delta\rvert$ (s)	Φ (s)
	960.53	3.68	967.199	2	38	6.672	
	1011.39	2.54	1013.941	2	40	2.551	
	1040.07	3.34	1038.204	2	41	1.866	
	1066.73	2.21	1066.513	1	24	0.217	
	1091.09	2.36	1084.277	2	43	6.813	
	1143.96	2.50	1148.820	1	26	4.860	
G255−2	685.00	44	685.022	1	13	0.225	0.120
	830.00	38	830.218	1	16	0.218	
HLTau−76	382.47	16.47	386.470	1	6	4.001	2.189
	449.12	6.7	447.284	2	14	1.836	
	492.12	7.12	494.302	1	8	2.182	
	540.95	28.45	540.790	2	18	0.160	
	596.79	14.40	595.623	1	10	1.167	
	664.21	14.94	663.649	1	12	0.561	
	781.00	9.1	789.047	2	27	8.047	
	799.10	5.91	799.328	1	15	0.228	
	933.64	2.40	933.879	1	18	0.239	
	976.64	6.46	977.320	2	34	0.680	
	1064.91	11.30	1064.845	1	21	0.065	
	1390.84	3.92	1389.281	1	28	1.559	
G232−38	741.60	1.9	741.121	1	14	0.479	2.155
	984.00	2.2	983.679	1	19	0.321	
	1147.50	1.9	1153.164	1	23	5.664	
G30−20	1068.00	13.8	1068.028	1	20	0.028	0.028

[a]Bognár & Paparó (2010), [b]Yeates et al. (2005), [c]Bischoff-Kim (2009), [d]Vauclair et al. (2000), [e]Voss et al. (2006), [f]Pakštienė et al. (2011), [g]Bognár et al. (2009), [h]Bradley (1995).

column of Table 5 shows the theoretical periods of the adopted asteroseismological model for each star, whereas the fifth and sixth columns include the ℓ- and k-identification, respectively, of each pulsation mode. The seventh column shows the absolute difference between observed and theoretical periods, and the eighth column indicates the value of the quality function defined by equation (1).

Below, we describe the general criteria adopted to choose the asteroseismological model for each star.

4.3.1 Criteria used in the fits

Usually, when performing period-to-period fits to ZZ Ceti stars, we found multiple seismological solutions, that is, many stellar models that nearly reproduce the periods observed in a given DAV star. So, in order to isolate a single asteroseismological model among the several possible and equally valid ones, we must apply some criteria.

(i) First, we looked for the models associated to the lowest value of the quality functions, thus ensuring that the observed periods are closely matched by the theoretical ones.

(ii) When possible, we used the external ℓ-identifications of the observed periods according to studies that employ the high-speed photometry method (see e.g. Robinson et al. 1995), the time-resolved ultraviolet spectroscopy method (see e.g. Kepler et al. 2000) or the time-resolved optical spectroscopy approach (see, e.g. Clemens, van Kerkwijk & Wu 2000).

(iii) When several families of solutions were found, we elected the models with values of $T_{\rm eff}$ and $\log g$ as close as possible to the spectroscopic ones. In this way, we guarantee that the surface parameters of the asteroseismological solutions are not in conflict with observations.

(iv) Among possible asteroseismological solutions with similar values of the quality function, we prioritized the solutions that fit the largest amplitude modes with theoretical modes having $\ell = 1$. This is because the well-known property that $\ell = 1$ modes exhibit substantially larger amplitudes than $\ell = 2$ ones, because geometric cancellation effects become increasingly severe as ℓ increases (Dziembowski 1977).

(v) In the cases in which several modes had similar amplitudes in the power spectrum, we gave more weight to stellar models that fit those periods with theoretical periods having the same ℓ value. In this way, we are assuming that two eigenmodes with different values of the harmonic degree ℓ usually should not have similar amplitudes.

(vi) For a given star showing a large number of modes, we favoured the seismological solutions that fit to observed periods with a larger number of $\ell = 1$ than $\ell = 2$ modes. This is because there is more chance to observe $\ell = 1$ modes than $\ell = 2$ modes.

(vii) In the opposite case, for stars exhibiting just a single period, we employed only the set of $\ell = 1$ periods to perform the period fit. Then, we chosen the asteroseismological model by searching for that model having the minimum value of the quality function, and we restricted the solutions by using the spectroscopic constraints ($T_{\rm eff}$ and $\log g$), if necessary.

4.3.2 Some particular cases

Because the large number of ZZ Ceti stars seismologically analysed in this work, it would be unpractical and tedious to describe in detail the procedure we followed to arrive at the asteroseismological model for each star, as we already did for the particular case of G117−B15A. Instead, we briefly summarize below a few details related to the selection process of the best-fitting model for some cases of interest. The structural parameters of the asteroseismological models for the complete set of ZZ Ceti stars analysed in this study are shown in Table 6.

G226−29. G226−29 also exhibits a single mode with a short period. Fortunately, there exist a robust constraint on its ℓ-identification. In fact, Kepler et al. (2005b) found that the mode is actually a triplet ($\ell = 1$) with the central component at a period of 109.278 s. The solution in this case corresponds to a rather massive model with a thick H envelope ($M_* \sim 0.77\,{\rm M}_\odot$, $M_{\rm H} = 2.02 \times 10^{-5} M_*$), in line with the spectroscopic observations.

HS 1531+7436. This star also exhibits a single mode with a very short period (for ZZ Ceti standards) at 112.5 s. Unfortunately, the presence of just one period turns very difficult any attempt of asteroseismology on this star, and we are forced to make a somewhat arbitrary assumption. If we assume that this mode corresponds to a $(\ell, k) = (1, 1)$ identification, then the stellar mass of the seismological model must be larger than $0.705\,{\rm M}_\odot$. In the first attempt to fit its periods, we obtained massive solutions ($M_* \sim 0.77\,{\rm M}_\odot$), but at effective temperatures excessively low ($\sim$10 800 K). These solutions are characterized by thick H envelopes. Since we have just a single observed period, it is possible to find a model with the appropriate H envelope thickness as to allow to fit the period at an effective temperature in close agreement with the spectroscopic value of $T_{\rm eff}$. To this end, we selected the sequence with

Table 6. Structural parameters of the asteroseismological models for the sample of ZZ Ceti stars analysed in this paper. The quoted uncertainties are the internal errors of our asteroseismic procedure.

Star	$\log g$	$T_{\rm eff}$ (K)	$M_*/{\rm M}_\odot$	$M_{\rm H}/M_*$	$M_{\rm He}/M_*$	$\log(L/{\rm L}_\odot)$	$\log(R/{\rm R}_\odot)$	$X_{\rm C}$	$X_{\rm O}$
HS 1531+7436	8.28 ± 0.06	$12\,496 \pm 210$	0.770 ± 0.034	$(1.55 \pm 0.23) \times 10^{-5}$	5.96×10^{-3}	-2.616 ± 0.011	-1.977 ± 0.011	0.332	0.655
GD 244	7.97 ± 0.04	$12\,422 \pm 105$	0.593 ± 0.012	$(1.17 \pm 0.36) \times 10^{-4}$	2.38×10^{-2}	-2.433 ± 0.011	-1.881 ± 0.011	0.283	0.704
G226−29	8.28 ± 0.06	$12\,270 \pm 290$	0.770 ± 0.034	$(2.02 \pm 0.31) \times 10^{-5}$	5.95×10^{-2}	-2.647 ± 0.011	-1.977 ± 0.011	0.332	0.655
HS 0507+0434B	8.10 ± 0.06	$12\,257 \pm 135$	0.660 ± 0.023	$(5.68 \pm 1.94) \times 10^{-5}$	1.21×10^{-2}	-2.532 ± 0.021	-1.918 ± 0.016	0.258	0.729
LP 133−144	8.03 ± 0.04	$12\,210 \pm 180$	0.609 ± 0.012	$(1.10 \pm 0.79) \times 10^{-6}$	2.45×10^{-2}	-2.507 ± 0.010	-1.903 ± 0.011	0.264	0.723
EC 11507−1519	8.17 ± 0.07	$12\,178 \pm 230$	0.705 ± 0.033	$(3.59 \pm 1.09) \times 10^{-5}$	7.63×10^{-3}	-2.592 ± 0.021	-1.943 ± 0.016	0.326	0.661
L19−2	8.17 ± 0.07	$12\,105 \pm 360$	0.705 ± 0.033	$(3.59 \pm 1.66) \times 10^{-5}$	7.63×10^{-3}	-2.602 ± 0.021	-1.943 ± 0.016	0.326	0.661
GD 66	8.01 ± 0.04	$12\,068 \pm 125$	0.593 ± 0.012	$(4.65 \pm 4.37) \times 10^{-7}$	2.39×10^{-2}	-2.514 ± 0.010	-1.896 ± 0.011	0.213	0.704
G132−12	7.96 ± 0.05	$12\,067 \pm 180$	0.570 ± 0.012	$(1.97 \pm 0.46) \times 10^{-6}$	3.49×10^{-2}	-2.486 ± 0.017	-1.882 ± 0.014	0.301	0.606
G207−9	8.40 ± 0.07	$12\,029 \pm 130$	0.837 ± 0.034	$(4.32 \pm 3.50) \times 10^{-7}$	3.19×10^{-3}	-2.761 ± 0.020	-2.017 ± 0.016	0.346	0.641
G117−B15A	8.00 ± 0.09	$11\,985 \pm 200$	0.593 ± 0.007	$(1.25 \pm 0.70) \times 10^{-6}$	2.39×10^{-2}	-2.497 ± 0.030	-1.882 ± 0.029	0.283	0.704
MCT 2148−2911	8.05 ± 0.04	$11\,851 \pm 150$	0.632 ± 0.014	$(7.58 \pm 1.79) \times 10^{-5}$	1.75×10^{-2}	-2.561 ± 0.011	-1.904 ± 0.011	0.232	0.755
G38−29	8.28 ± 0.06	$11\,818 \pm 50$	0.770 ± 0.034	$(1.23 \pm 0.76) \times 10^{-5}$	5.96×10^{-3}	-2.716 ± 0.011	-1.979 ± 0.010	0.333	0.655
PG 1541+650	8.04 ± 0.04	$11\,761 \pm 60$	0.609 ± 0.012	$(1.56 \pm 1.42) \times 10^{-9}$	2.46×10^{-2}	-2.583 ± 0.010	-1.908 ± 0.011	0.264	0.723
G191−16	8.06 ± 0.04	$11\,741 \pm 90$	0.632 ± 0.014	$(1.39 \pm 0.32) \times 10^{-5}$	1.76×10^{-2}	-2.590 ± 0.010	-1.910 ± 0.011	0.232	0.755
G185−32	8.12 ± 0.10	$11\,721 \pm 370$	0.660 ± 0.023	$(4.46 \pm 3.20) \times 10^{-7}$	1.22×10^{-2}	-2.632 ± 0.051	-1.930 ± 0.034	0.258	0.729
EC 14012−1446	8.05 ± 0.04	$11\,709 \pm 95$	0.632 ± 0.014	$(7.58 \pm 2.40) \times 10^{-5}$	1.75×10^{-2}	-2.583 ± 0.011	-1.904 ± 0.011	0.232	0.755
EC 23487−2424	8.28 ± 0.06	$11\,700 \pm 75$	0.770 ± 0.034	$(2.02 \pm 0.32) \times 10^{-5}$	5.95×10^{-3}	-2.731 ± 0.010	-1.978 ± 0.010	0.332	0.655
GD 165	8.05 ± 0.07	$11\,635 \pm 330$	0.632 ± 0.014	$(7.58 \pm 3.28) \times 10^{-5}$	1.75×10^{-2}	-2.594 ± 0.043	-1.904 ± 0.029	0.232	0.755
R548	8.03 ± 0.05	$11\,627 \pm 390$	0.609 ± 0.012	$(1.10 \pm 0.38) \times 10^{-6}$	2.45×10^{-2}	-2.594 ± 0.025	-1.904 ± 0.015	0.264	0.723
HE 1258+0123	8.07 ± 0.03	$11\,582 \pm 100$	0.632 ± 0.014	$(4.46 \pm 3.07) \times 10^{-6}$	1.76×10^{-2}	-2.620 ± 0.014	-1.913 ± 0.007	0.232	0.755
GD 154	8.20 ± 0.04	$11\,574 \pm 30$	0.705 ± 0.033	$(4.58 \pm 1.80) \times 10^{-10}$	7.66×10^{-3}	-2.705 ± 0.003	-1.955 ± 0.003	0.326	0.661
GD 385	8.07 ± 0.03	$11\,570 \pm 90$	0.632 ± 0.014	$(4.59 \pm 2.86) \times 10^{-7}$	1.76×10^{-2}	-2.628 ± 0.005	-1.962 ± 0.005	0.232	0.755
HE 1429−037	8.13 ± 0.05	$11\,535 \pm 85$	0.660 ± 0.023	$(4.68 \pm 0.86) \times 10^{-10}$	1.22×10^{-3}	-2.667 ± 0.018	-1.934 ± 0.013	0.258	0.729
HS 1249+0426	8.02 ± 0.02	$11\,521 \pm 35$	0.609 ± 0.012	$(3.53 \pm 1.08) \times 10^{-5}$	2.45×10^{-2}	-2.595 ± 0.002	-1.896 ± 0.002	0.264	0.723
G238−53	8.03 ± 0.02	$11\,497 \pm 120$	0.609 ± 0.012	$(1.54 \pm 0.28) \times 10^{-6}$	2.46×10^{-2}	-2.613 ± 0.002	-1.904 ± 0.002	0.264	0.723
HS 1625+1231	8.02 ± 0.04	$11\,485 \pm 230$	0.609 ± 0.012	$(3.52 \pm 1.67) \times 10^{-5}$	2.45×10^{-2}	-2.600 ± 0.016	-1.896 ± 0.012	0.264	0.723
G29−38	8.01 ± 0.03	$11\,471 \pm 60$	0.593 ± 0.012	$(4.67 \pm 2.83) \times 10^{-10}$	2.39×10^{-2}	-2.612 ± 0.006	-1.901 ± 0.006	0.283	0.704
PG 2303+242	7.88 ± 0.07	$11\,210 \pm 100$	0.525 ± 0.12	$(4.54 \pm 2.95) \times 10^{-8}$	4.94×10^{-2}	-2.579 ± 0.03	-1.865 ± 0.032	0.279	0.709
MCT 0145−2211	7.95 ± 0.03	$11\,439 \pm 120$	0.570 ± 0.012	$(1.43 \pm 0.38) \times 10^{-5}$	3.50×10^{-2}	-2.573 ± 0.014	-1.879 ± 0.012	0.301	0.686
BPM 30551	8.19 ± 0.05	$11\,435 \pm 40$	0.705 ± 0.033	$(4.36 \pm 0.26) \times 10^{-6}$	7.66×10^{-3}	-2.714 ± 0.006	-1.949 ± 0.006	0.326	0.661
GD 99	8.01 ± 0.13	$11\,395 \pm 25$	0.660 ± 0.023	$(1.36 \pm 0.52) \times 10^{-5}$	1.22×10^{-2}	-2.671 ± 0.005	-1.950 ± 0.068	0.258	0.729
BPM 24754	8.03 ± 0.03	$11\,390 \pm 50$	0.609 ± 0.012	$(4.51 \pm 2.72) \times 10^{-6}$	2.46×10^{-2}	-2.626 ± 0.011	-1.902 ± 0.001	0.264	0.723
KUV 02464+3239	7.93 ± 0.03	$11\,360 \pm 40$	0.548 ± 0.014	$(4.71 \pm 2.45) \times 10^{-8}$	4.21×10^{-2}	-2.579 ± 0.006	-1.876 ± 0.006	0.290	0.697
PG 1149+058	7.94 ± 0.02	$11\,336 \pm 20$	0.570 ± 0.012	$(5.29 \pm 2.45) \times 10^{-5}$	3.69×10^{-2}	-2.579 ± 0.001	-1.875 ± 0.002	0.301	0.686
BPM 31594	7.86 ± 0.03	$11\,250 \pm 70$	0.525 ± 0.012	$(5.36 \pm 1.87) \times 10^{-5}$	4.93×10^{-2}	-2.545 ± 0.009	-1.851 ± 0.009	0.279	0.709
KUV 11370+4222	8.06 ± 0.03	$11\,237 \pm 80$	0.632 ± 0.014	$(1.40 \pm 0.64) \times 10^{-5}$	1.76×10^{-2}	-2.668 ± 0.007	-1.911 ± 0.008	0.232	0.755
HS 1824−6000	7.95 ± 0.08	$11\,234 \pm 400$	0.570 ± 0.012	$(1.43 \pm 0.62) \times 10^{-5}$	3.50×10^{-2}	-2.605 ± 0.050	-1.879 ± 0.030	0.301	0.686
KUV 08368+4026	8.02 ± 0.03	$11\,230 \pm 95$	0.609 ± 0.012	$(1.42 \pm 0.52) \times 10^{-5}$	2.45×10^{-2}	-2.646 ± 0.010	-1.899 ± 0.007	0.264	0.723
R808	8.18 ± 0.05	$11\,213 \pm 130$	0.705 ± 0.033	$(3.59 \pm 1.70) \times 10^{-5}$	7.63×10^{-3}	-2.738 ± 0.008	-1.944 ± 0.008	0.326	0.661
G255−2	8.11 ± 0.04	$11\,185 \pm 30$	0.660 ± 0.023	$(4.45 \pm 2.12) \times 10^{-6}$	1.22×10^{-2}	-2.709 ± 0.002	-1.928 ± 0.003	0.258	0.729
HLTau−76	7.89 ± 0.03	$11\,111 \pm 50$	0.548 ± 0.012	$(1.83 \pm 1.03) \times 10^{-4}$	4.19×10^{-2}	-2.579 ± 0.005	-1.857 ± 0.005	0.323	0.697
G232−38	7.99 ± 0.04	$10\,952 \pm 120$	0.593 ± 0.012	$(5.19 \pm 1.87) \times 10^{-5}$	2.38×10^{-2}	-2.666 ± 0.015	-1.888 ± 0.010	0.283	0.704
G30−20	7.91 ± 0.02	$10\,950 \pm 15$	0.548 ± 0.012	$(5.34 \pm 2.18) \times 10^{-5}$	4.20×10^{-2}	-2.618 ± 0.002	-1.863 ± 0.002	0.290	0.697

$M_* = 0.77\,{\rm M}_\odot$ and computed an additional sequence with $M_{\rm H} = 1.55 \times 10^{-5} M_*$. In this way, we obtained a best-fitting model with $T_{\rm eff} \simeq 12\,350$ K.

G185−32. The pulsation spectrum of this DAV includes a period at 215.74 s, quite similar to the dominant mode in G117−B15A, but at variance with this star, the difference of amplitude between this mode and the remaining ones is not so strong in the case of G185−32. The identification of the ℓ degree for the periodicities observed in G185−32 is not well determined. In particular, the period at ∼215 s is associated with a $\ell = 1$ or 2 mode (Castanheira et al. 2004; Yeates et al. 2005). Similarly to G117−B15A, for this star the stellar models fit the period at 215.74 s with a mode characterized by $\ell = 1$ and $k = 2$. However, the seismological model for this star is more massive than in the case of G117−B15A. For G185−32 we adopted an asteroseismological model that closely fit the period at ∼215 and at the same time it matches the set of observed periods with mostly $\ell = 1$ modes.

GD 154. This star shows three pulsation modes. The mode with period at 402.6 s is a unstable and low amplitude mode, as compared with the remaining two modes (Pfeiffer et al. 1996). Since the amplitude of the long-period modes (1088.6 and 1186.5 s) is very similar, and since the period at 1186.5 s is probably a dipole mode (Pfeiffer et al. 1996) we favour models that fit these periods with $\ell = 1$ modes. Generally, the solutions have a stellar mass between 0.6323 and 0.705 $\rm M_\odot$ with thin H envelopes ($M_{\rm H} \sim 10^{-8} - 10^{-10} M_*$). Among them, we choose the solution with $M_* = 0.705\,{\rm M}_\odot$ and $M_{\rm H} = 4.58 \times 10^{-10} M_*$ because it has surface parameters in agreement with spectroscopy. Other similar solutions have $T_{\rm eff} \sim 11\,200$ K, but in these cases the period at 402.6 s is identified with $\ell = 2$.

G238−53, G132−12 and LP 133−144. These three stars also have a period near 215 s. In all the cases, this mode has an identification $k = 2$ when $\ell = 1$. This ℓ and k identification is an intrinsic property shared by all the asteroseismological models of this study. This can be seen from Fig. 6, that shows that the periods with $\ell = 1$ and $k = 1$ are always too short to match the ∼215 s period.

R548. This star has a slightly higher effective temperature and a spectroscopic stellar mass a bit larger than G117−B15A. Frequently, both stars are analysed together due to these similarities and several periods in common. In the first attempts to fit the periods of R548 we obtained solutions with high mass, but were discarded because the 212 s periods was identified with $\ell = 2$ according to those models. Also, intermediate mass solutions were obtained. Generally, the modes with periods at 318.07 and 333.64 s are the most poorly matched by the models, and they are identified with $\ell = 2$. In order to found a best-fitting model for this star, we were forced to employ several restrictions. We assumed that the mode with the period at 212.95 s has $\ell = 1$ and $k = 2$, and fixed $\ell = 1$ also for the mode with the period at 274.272 s (Yeates et al. 2005). We found an asteroseismological model with $M_* = 0.609\,\mathrm{M}_\odot$, larger than the stellar mass obtained for G117−B15A ($M_* = 0.593\,\mathrm{M}_\odot$) and a $T_{\rm eff}$ lower, in contrast to the trend indicated by spectroscopy and by the previous studies (Bradley 1998; Castanheira & Kepler 2009). However, the surface parameters characterizing the best-fitting model are within the uncertainties of spectroscopy.

MCT 2148−2911, PG 1541+650, HE 1429−037 and HS 1824−600. These are low-mass white dwarfs, with spectroscopic masses of 0.515, 0.502, 0.514 and 0.427 $\mathrm{M}_\odot$, respectively. These values are obtained by extrapolation from our evolutionary model grid. However, our asteroseismological models for these stars do not have the lowest mass of our model grid (0.525 $\mathrm{M}_\odot$), but instead, they result in intermediate masses: 0.632, 0.609, 0.660 and 0.570 $\mathrm{M}_\odot$, respectively. The $T_{\rm eff}$ values of these models are in agreement with the spectroscopic inferences.

GD 244. For this star we have not been able to found any plausible seismological model with an effective temperature close to the spectroscopic value ($T_{\rm eff} = 11\,680$ K). In order to adopt a seismological model, we considered that the large amplitude modes are $\ell = 1$, and found an acceptable solution with a $T_{\rm eff} = 12\,422$ K, markedly higher than the spectroscopic one. On the other hand, the gravity and stellar mass of the adopted seismological model are compatible (within the uncertainties) with the spectroscopic estimates.

G207−9. For this DAV we obtain a massive seismological solution, with $M_* = 0.837\,\mathrm{M}_\odot$. However, a second solution, although with a slightly worse period match, according to $\Phi = 1.496$ s, is obtained for a lower mass ($M_* = 0.609\,\mathrm{M}_\odot$), characterized by a thick H envelope ($M_{\rm H} = 1.41 \times 10^{-5} M_*$). A degeneracy of solutions for this star has been also found by Castanheira & Kepler (2009).

G29−38. This is a rather pathological case. In spite of the fact that this star has $T_{\rm eff} \sim 11\,800$ K, it exhibits a rich and complex period spectrum (including 14 genuine eigenmodes) which is characteristic of cooler DAVs. Thompson, van Kerkwijk & Clemens (2008), by means of Very Large Telescope (VLT) spectroscopy, show that most of the periodicities exhibited by this star are $\ell = 1$ modes, but there are also some $\ell = 2$ modes and possibly one mode with $\ell = 3$ or 4. However, the seismological solutions for this star imply that most of the observed modes should be $\ell = 2$. In the asteroseismological model adopted, the only $\ell = 1$ mode is associated to the mode with a period 614.4 s which has the largest amplitude.

PG 2303−243. For this star, the observed modes and amplitudes were taken from Pakštienė et al. (2011). These authors show that this ZZ Ceti has a very rich pulsation spectrum with 24 probably independent modes. However, most of these modes show very low amplitudes, below ∼4 mma. In our analysis, we considered to be real modes only those showing amplitudes higher than ∼4 mma, leaving us with just four periodicities. In particular, we fixed the harmonic degree to be $\ell = 1$ for the two main modes, 616.4 and 965.3 s, while we allow the remainder modes to be $\ell = 1$ or 2.

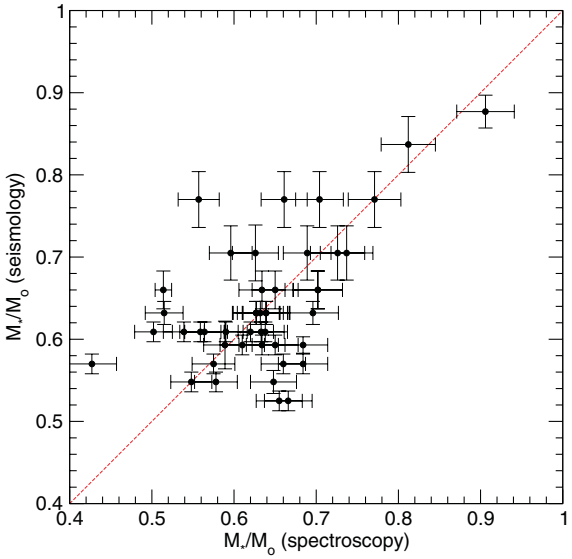

Figure 9. Comparison between the value of the stellar mass of the 44 DAVs stars analysed in this work, according to our spectroscopic inference (x-axis) and from our asteroseismological analysis (y-axis). The red dashed line represents a perfect match between both mass estimates.

4.3.3 *Seismic stellar masses*

In this work, the DA white dwarf evolutionary tracks used to derive the spectroscopic masses of the DAVs have been employed to infer the asteroseismological masses. Thus, a comparison between both sets of values is worth doing. We compare in Fig. 9 the spectroscopic and asteroseismological masses. The dotted line is the 1:1 correspondence. The plot reveals that the general agreement between both sets of estimations is far from being good, the larger discrepancies reaching differences up to ∼0.2 $\mathrm{M}_\odot$. However, the bulk of the points in Fig. 9 accumulate around the dotted line, demonstrating that no appreciable offset exists between the spectroscopic and asteroseismic estimations of the stellar mass.

The distribution of stellar masses according to asteroseismology and spectroscopy is depicted in the histograms of the upper and lower panel of Fig. 10, respectively. The mean value of the asteroseismological mass is $\langle M_* \rangle_{\rm seis} = 0.636 \pm 0.019\,\mathrm{M}_\odot$, slightly larger (∼0.95 per cent) than the spectroscopic one, $\langle M_* \rangle_{\rm spec} = 0.630 \pm 0.028\,\mathrm{M}_\odot$.[2] Given the very different methods employed to infer both values, the excellent agreement between these average masses is encouraging.

Castanheira & Kepler (2008, 2009) have performed the first asteroseismological study of an ensemble of ZZ Ceti stars. They have studied a total of 83 ZZ Ceti stars including the bright variables and also a subset of the SDSS variables. The average mass of the

[2] We do not claim the pulsators are more massive, as there are strong selection effects in the search for pulsators.

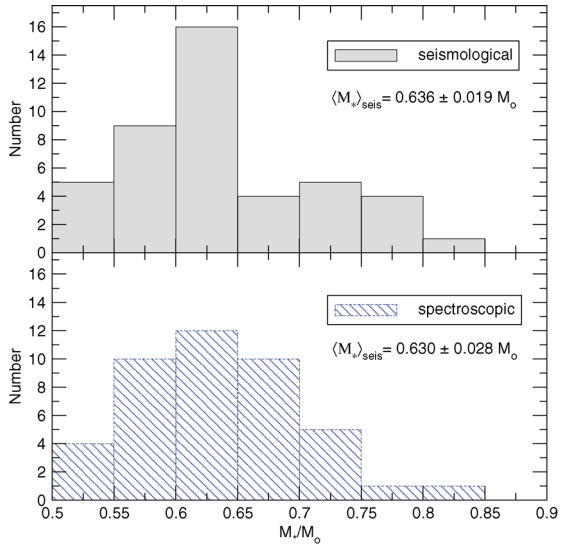

Figure 10. Histograms showing the mass distribution for the sample of 44 ZZ Ceti stars considered in this work, according to our spectroscopic inferences (lower panel) and our seismological analysis (upper panel).

ZZ Ceti stars as derived by these authors is $\langle M_*\rangle_{\rm seis} = 0.668\,{\rm M}_\odot$, about 5 per cent higher than our value, $\langle M_*\rangle_{\rm seis} = 0.636\,{\rm M}_\odot$. We note that Castanheira & Kepler (2008, 2009) have included several very massive ZZ Ceti stars ($M_* \gtrsim 1\,{\rm M}_\odot$) that have not been considered in our study. Given the fact that the numerical tools used in modelling the structure, evolution and pulsations of ZZ Ceti stars used by the two groups are independent, and given that the samples of stars analysed are not the same, we consider that the $\langle M_*\rangle_{\rm seis}$ value derived in this work and that derived by Castanheira & Kepler (2008, 2009) are in very good agreement.

4.3.4 The thicknesses of the hydrogen envelope

One of the most important structural parameters we want to constrain through asteroseismology of ZZ Ceti stars is the thickness of the H envelope in DA white dwarfs. We have found a H layer mass of $M_{\rm H} = (1.25 \pm 0.7) \times 10^{-6} M_*$ for G117−B15A, about two order of magnitude thinner than the value predicted by canonical evolutionary computations, of $M_{\rm H} \sim 10^{-4} M_*$. Here, the analysis of a large number of ZZ Ceti stars allows us to explore the distribution of H envelope thicknesses from their pulsations. In Fig. 11 we present histograms of the distribution of H envelope thicknesses. In the upper panel we show the results for the complete sample of 44 stars. Note that there is a pronounced maximum of the distribution for $\log(M_{\rm H}/M_*)$ in the range -5 to -4, although there exists another, much less notorious maximum for $\log(M_{\rm H}/M_*)$ between -10 and -9. So, it is apparent from the figure that there exists a *range* of thicknesses of the H envelope in the studied DAV stars, with a strong peak at thick envelopes and another much lower peak at very thin envelopes, and an apparent paucity for intermediate thicknesses. In the middle panel of Fig. 11 we show the histogram corresponding to the asteroseismological models characterized by canonical (thick) H envelope thicknesses, that amount to 11 stars. Finally, in the lower panel we display the histogram for the non-canonical thicknesses, that is, envelopes thinner than those predicted by standard evolutionary computations depending on the value of the stellar mass. As in previous sections, we refer this kind of envelopes as 'thin' envelopes. We recall that these 'thin' envelopes have been generated in this work in order to extend the exploration of the parameter space of the models for asteroseismology. Note that in most of the analysed stars (34 stars from a total of 44) our asteroseismological models have 'thin' H envelopes, as illustrated in Fig. 12. It is important to note, however, that most of our derived envelope masses, even being thinner than the canonical values, cluster close to the envelope masses predicted by standard evolutionary computations, at variance with those of Castanheira & Kepler (2009), who found

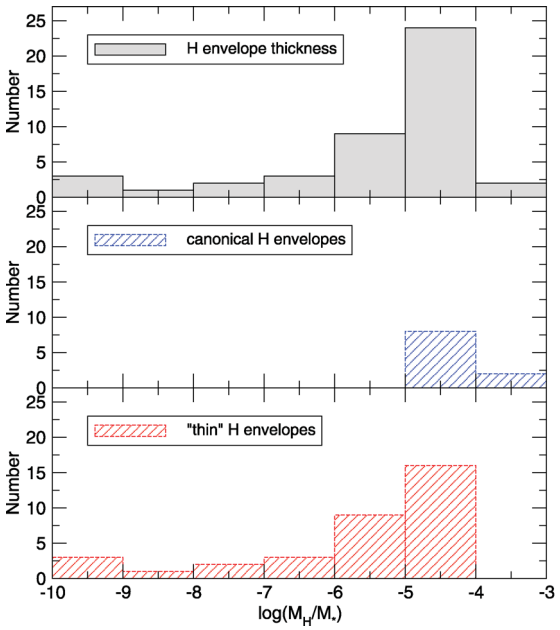

Figure 11. Upper panel: histogram showing the H envelope thickness distribution for the sample of 44 ZZ Ceti stars considered in this work. Middle panel: histogram for models with canonical (thick) H envelope thicknesses, as predicted by canonical evolutionary computations according to the value of the stellar mass. Lower panel: histogram for models with non-canonical (thin) envelope thicknesses, as obtained by means of our artificial procedure described in Section 2.3.

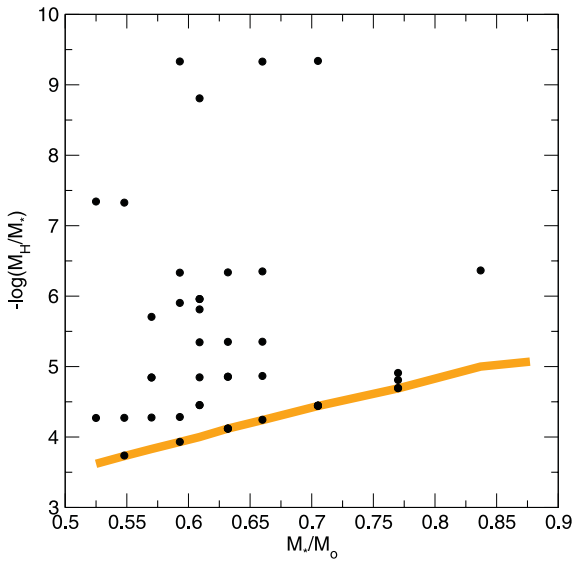

Figure 12. The values of the H envelope mass versus the stellar mass corresponding to the asteroseismological models of the 44 ZZ Ceti stars analysed in this work. The thick (orange) curve depicts the canonical values for the H envelope thickness.

a nearly homogeneous distribution of envelope masses in their fits (see their fig. 8).

The mean value of the H layer mass is $\langle M_{\rm H}/M_*\rangle = 2.71 \times 10^{-5}$ according to our results. This value is about 50 times larger than the value obtained by Castanheira & Kepler (2009) with different samples, $\langle M_{\rm H}/M_*\rangle = 5.01 \times 10^{-7}$. In spite of this difference, both studies concur to the conclusion that an important fraction of DA white dwarfs might have been formed with a H mass smaller than the value predicted by standard evolutionary computations, a conclusion we have already suggested at end of Section 4.2 on the basis of our results on G117−B15A.

5 CONCLUSIONS

In this paper, we have carried out the first asteroseismological application of the evolutionary DA white dwarf models presented in Althaus et al. (2010b).[3] Specifically, we performed a detailed asteroseismological study of 44 ZZ Ceti stars extracted from a sample of bright stars for which the surface parameters are accurately known. This sample includes the archetypal ZZ Ceti star G117−B15A. The asteroseismological analysis of such a large set of stars has the potential to characterize the common properties of the class. We have employed a large grid of fully evolutionary models characterized by consistent chemical profiles from the centre to the surface and covering a wide range of stellar masses, thicknesses of the H envelope and effective temperatures. Our asteroseismological approach represents a significant improvement over previous calculations that rely on the use of DA white dwarf models characterized by simplified chemical profiles at the envelope and/or the core. This is the first work aimed at an asteroseismological analysis of ZZ Ceti stars that employs *fully evolutionary* white dwarf models.

Our main results for G117−B15A are the following.

(i) We found an asteroseismological model for G117−B15A with $T_{\rm eff} = 11\,985 \pm 200$ K, $\log g = 8.00 \pm 0.09$ and $M_* = 0.593 \pm 0.007\,{\rm M}_\odot$, in excellent agreement with the spectroscopic determinations.

(ii) For the first time, we break the degeneracy of the asteroseismological solutions for this star reported by previous studies regarding the thickness of the H envelope, depending on the k-identification of the three periods exhibited by G117−B15A, although it is fair to say that we are matching three periods by varying three parameters. We found the identification $k = 2, 3, 4$ as the only possible one in the frame of our set of pulsation models.

(iii) Our best-fitting model has a H envelope with $M_{\rm H} = (1.25 \pm 0.7) \times 10^{-6} M_*$, about two order of magnitude thinner than the value predicted by canonical evolutionary computations, of $M_{\rm H} \sim 10^{-4} M_*$ at this stellar mass value.

(iv) The value of the thickness of the H envelope of our best-fitting model is in perfect agreement with the predictions of the post-LTP scenario proposed by Althaus et al. (2005) for the formation of DA white dwarfs with thin H envelopes.

(v) The luminosity of our asteroseismological model allows us to infer a seismological parallax of G117−B15A, that is substantially larger than its trigonometric parallax. In agreement with previous works, we argue that the trigonometric parallax uncertainty is larger and the seismological derivation of the parallax is robust.

[3] Detailed tabulations of the chemical profiles for different stellar masses and effective temperatures are available at our web site http://www.fcaglp.unlp.edu.ar/evolgroup

As for the complete sample of 44 ZZ Ceti stars, our main results are the following.

(i) We determined the spectroscopic masses of the 44 stars analysed using our DA white dwarf evolutionary tracks.

(ii) The mean value of the asteroseismological mass is $\langle M_*\rangle_{\rm seis} = 0.636 \pm 0.019\,{\rm M}_\odot$, slightly higher than our mean spectroscopic mass, of $\langle M_*\rangle_{\rm spec} = 0.630 \pm 0.028\,{\rm M}_\odot$. Given the completely different approaches employed to derive both values, the agreement can be considered as excellent.

(iii) Our derived value for $\langle M_*\rangle_{\rm seis}$ is in line with the mean mass of DA white dwarfs inferred by Tremblay et al. (2011), $\langle M_*\rangle_{\rm DA} = 0.613\,{\rm M}_\odot$, and in good agreement with the value derived by Falcon et al. (2010), $\langle M_*\rangle_{\rm DA} = 0.647^{+0.013}_{-0.014}\,{\rm M}_\odot$.

(iv) There exists a range of thicknesses of the H envelope in the studied ZZ Ceti stars, in qualitative agreement with the results of Castanheira & Kepler (2009). Our distribution of H envelope thicknesses is characterized by a strong peak at thick envelopes [$\log (M_{\rm H}/M_*) \sim -4.5$] and another much less pronounced peak at very thin envelopes [$\log (M_{\rm H}/M_*) \sim -9.5$], with an evident paucity for intermediate thicknesses.

(v) In most of the analysed DAVs (34 stars from a total of 44), our asteroseismological models have H envelopes thinner than the values predicted by standard evolutionary computations for a given stellar mass. However, our envelope masses cluster closer to the canonical envelope masses than those of Castanheira & Kepler (2009).

In closing, we note that Tremblay & Bergeron (2008) have studied the ratio of He- to H-rich white dwarfs in terms of $T_{\rm eff}$ from a model atmosphere analysis of the infrared photometric data from the Two Micron All Sky Survey combined with available visual magnitudes. They found that this ratio increases gradually from $\approx$0.25 for $15\,000 \gtrsim T_{\rm eff} \gtrsim 10\,000$ K to about 0.5 for $10\,000 \gtrsim T_{\rm eff} \gtrsim 8000$ K due to convective mixing when the bottom of the H convection zone reaches the underlying convective He envelope. These authors conclude that about 15 per cent of the DA white dwarfs should have H envelopes with $\log (M_{\rm H}/M_*)$ between -10 and -8. The asteroseismological results reported in this work point to the existence of large fraction of DAV stars with H envelopes thinner than canonical values. In particular, five ZZ Ceti stars analysed have $10^{-10} \lesssim M_{\rm H}/M_* \lesssim 10^{-8}$, which represents the 11 per cent of the sample of the studied DAV stars. This fraction of stars with very thin H envelopes is compatible with the results of Tremblay & Bergeron (2008).

In a detailed asteroseismological analysis of an ensemble of ZZ Ceti stars, Castanheira & Kepler (2008, 2009) have found that the H envelope of these stars could be within the range $3 \times 10^{-10} \lesssim M_{\rm H}/M_* \lesssim 10^{-4}$, with an average value of $\langle M_{\rm H}/M_*\rangle = 5 \times 10^{-7}$. In many respects, the results of the present study are in excellent agreement with the predictions of Castanheira & Kepler (2008, 2009). Our different mean value for the H layer mass, $\langle M_{\rm H}/M_*\rangle = 2.71 \times 10^{-5}$, which is about 50 times larger than that found by those authors, could be due to the fact that our studies are based on completely independent sets of DA white dwarf models, different pulsational codes, and different samples of stars.

All these results reinforce the idea that a non-negligible fraction of DA white dwarfs with thin H envelopes could exist, rendering as a plausible one the scenario proposed by Althaus et al. (2005) for the formation of DA white dwarfs with $M_{\rm H}$ smaller than predicted by the standard theory. Hopefully, new asteroseismological analysis on a larger number of DAV stars, including the ZZ Ceti stars from the SDSS, based on fully evolutionary DA white dwarf models with

realistic chemical profiles like the ones employed in this work, will help to place this idea on a firmer basis.

ACKNOWLEDGMENTS

Part of this work was supported by AGENCIA through the Programa de Modernización Tecnológica BID 1728/OC-AR, by the PIP 112-200801-00940 grant from CONICET and CAPES/MINCyT. This research has made use of NASA's Astrophysics Data System.

REFERENCES

Aizenman M., Smeyers P., Weigert A., 1977, A&A, 58, 41
Allen C. W., 1973, Astrophysical Quantities, 3rd edn. Athlone Press, London
Althaus L. G., Serenelli A. M., Córsico A. H., Montgomery M. H., 2003, A&A, 404, 593
Althaus L. G., Miller Bertolami M. M., Córsico A. H., García-Berro E., Gil-Pons P., 2005, A&A, 440, L1
Althaus L. G., Córsico A. H., Isern J., García-Berro E., 2010a, A&AR, 18, 471
Althaus L. G., Córsico A. H., Bischoff-Kim A., Romero A. D., Renedo I., García-Berro E., Miller Bertolami M. M., 2010b, ApJ, 717, 897
Angulo C. et al., 1999, Nuclear Phys. A, 656, 3
Benvenuto O. G., Córsico A. H., Althaus L. G., Serenelli A. M., 2002, MNRAS, 332, 399
Bergeron P., Wesemael F., Beauchamp A., 1995a, PASP, 107, 1047
Bergeron P., Wesemael F., Lamontagne R., Fontaine G., Saffer R. A., Allard N. F., 1995b, ApJ, 449, 258
Bergeron P., Fontaine G., Billères M., Boudreault S., Green E. M., 2004, ApJ, 600, 404
Bischoff-Kim A., 2009, in Guzik J. A., Bradley P. A., eds, AIP Conf. Ser. Vol. 1170, Stellar Pulsations: Challenges for the Theory and Observations. Am. Inst. Phys., New York, p. 621
Bischoff-Kim A., Montgomery M. H., Winget D. E., 2008a, ApJ, 675, 1505
Bischoff-Kim A., Montgomery M. H., Winget D. E., 2008b, ApJ, 675, 1512
Blöcker T., 2001, Ap&SS, 275, 1
Bognár Z., Paparó M., 2010, in Werner K., Rauch T. eds, AIP Conf. Ser. Vol. 1273, 17th European white Dwarf Workshop. Am. Inst. Phys., New York, p. 504
Bognár Z., Paparó M., Bradley P. A., Bischoff-Kim A., 2009, MNRAS, 399, 1954
Bradley P. A., 1995, Baltic Astron., 4, 536
Bradley P. A., 1996, ApJ, 468, 350
Bradley P. A., 1998, ApJS, 116, 307
Brickhill A. J., 1991, MNRAS, 251, 673
Burgers J. M., 1969, Flow Equations for Composite Gases. Academic Press, New York
Castanheira B. G., Kepler S. O., 2008, MNRAS, 385, 430
Castanheira B. G., Kepler S. O., 2009, MNRAS, 396, 1709
Castanheira B. G. et al., 2004, A&A, 413, 623
Castanheira B. G. et al., 2006, A&A, 450, 227
Castanheira B. G. et al., 2007, A&A, 462, 989
Castanheira B. G., Kepler S. O., Kleinman S. J., Nitta A., Fraga L., 2010, MNRAS, 405, 2561
Caughlan G. R., Fowler W. A., Harris M. J., Zimmermann B. A., 1985, Atomic Data Nuclear Data Tables, 32, 197
Clemens J. C., van Kerkwijk M. H., Wu Y., 2000, MNRAS, 314, 220
Córsico A. H., Althaus L. G., 2006, A&A, 454, 863
Córsico A. H., Benvenuto O. G., Althaus L. G., Isern J., García-Berro E., 2001, New Astron., 6, 197
Córsico A. H., Benvenuto O. G., Althaus L. G., Serenelli A. M., 2002, MNRAS, 332, 392
Córsico A. H., García-Berro E., Althaus L. G., Isern J., 2004, A&A, 427, 923
Córsico A. H., Althaus L. G., Montgomery M. H., García-Berro E., Isern J., 2005, A&A, 429, 277
Córsico A. H., Althaus L. G., Miller Bertolami M. M., Werner K., 2007a, A&A, 461, 1095
Córsico A. H., Miller Bertolami M. M., Althaus L. G., Vauclair G., Werner K., 2007b, A&A, 475, 619
Córsico A. H., Althaus L. G., Kepler S. O., Costa J. E. S., Miller Bertolami M. M., 2008, A&A, 478, 869
Córsico A. H., Althaus L. G., Miller Bertolami M. M., García-Berro E., 2009, A&A, 499, 257
Córsico A. H., Althaus L. G., Romero A. D., Miller Bertolami M. M., García-Berro E., Isern J., 2011, in Shibahashi H., ed., ASP Proceedings of 61st Fujihara Seminar: Progress in Solar/Stellar Physics with Helio- and Asteroseismology, preprint (arXiv:1108.3541)
Dolez N., Vauclair G., 1981, A&A, 102, 375
Dziembowski W., 1971, Acta Astron., 21, 289
Dziembowski W., 1977, Acta Astron., 27, 203
Falcon R. E., Winget D. E., Montgomery M. H., Williams K. A., 2010, ApJ, 712, 585
Fontaine G., Brassard P., 2008, PASP, 120, 1043
Fontaine G., Bergeron P., Billères M., Charpinet S., 2003, ApJ, 591, 1184
Gianninas A., Bergeron P., Fontaine G., 2005, ApJ, 631, 1100
Gianninas A., Bergeron P., Fontaine G., 2006, AJ, 132, 831
Goldreich P., Wu Y., 1999, ApJ, 511, 904
Herwig F., Blöcker T., Schönberner D., El Eid M., 1997, A&A, 324, L81
Herwig F., Freytag B., Fuchs T., Hansen J. P., Hueckstaedt R. M., Porter D. H., Timmes F. X., Woodward P. R., 2007, in Kerschbaum F., Charbonnel C., Wing R. F., eds, ASP Conf. Ser. Vol. 378, Why Galaxies Care About AGB Stars: Their Importance as Actors and Probes. Astron. Soc. Pac., San Francisco, p. 43
Holberg J. B., Bergeron P., Gianninas A., 2008, AJ, 135, 1239
Homeier D., Koester D., Hagen H.-J., Jordan S., Heber U., Engels D., Reimers D., Dreizler S., 1998, A&A, 338, 563
Isern J., Hernanz M., García-Berro E., 1992, ApJ, 392, L23
Isern J., García-Berro E., Althaus L. G., Córsico A. H., 2010, A&A, 512, A86
Kanaan A. et al., 2005, A&A, 432, 219
Kepler S. O., Nather R. E., McGraw J. T., Robinson E. L., 1982, ApJ, 254, 676
Kepler S. O., Robinson E. L., Koester D., Clemens J. C., Nather R. E., Jiang X., 2000, ApJ, 539, 379
Kepler S. O. et al., 2005a, ApJ, 634, 1311
Kepler S. O., Castanheira B. G., Saraiva M. F. O., Nitta A., Kleinman S. J., Mullally F., Winget D. E., Eisenstein D. J., 2005b, A&A, 442, 629
Kepler S. O., Kleinman S. J., Pelisoli I., Pecana V., Diaz M., Koester D., Castanheira B. G., Nitta A., 2010, in Werner K., Rauch T., eds, AIP Conf. Ser. Vol. 1273, 17th European White Dwarf Workshop. Am. Inst. Phys., New York, p. 19
Koester D., Allard N. F., 2000, Baltic Astron., 9, 119
Koester D., Holberg J. B., 2001, in Provencal J. L., Shipman H. L., MacDonald J., Goodchild S., eds, ASP Conf. Ser. Vol. 226, 12th European Workshop on White Dwarfs. Astron. Soc. Pac., San Francisco, p. 299
Kotak R., van Kerkwijk M. H., Clemens J. C., 2004, A&A, 413, 301
Lugaro M., Herwig F., Lattanzio J. C., Gallino R., Straniero O., 2003, ApJ, 586, 1305
McGraw J. T., Robinson E. L., 1976, ApJ, 205, L155
Metcalfe T. S., Montgomery M. H., Kanaan A., 2004, ApJ, 605, L133
Miller Bertolami M. M., Alhaus L. G., Córsico A. H., 2005, Bol. Asociación Argentina Astron., 48, 185
Montgomery M. H., 2005a, ApJ, 633, 1142
Montgomery M. H., 2005b, in Koester D., Moehler S., eds, ASP Conf. Ser. Vol. 334, 14th European Workshop on White Dwarfs. Astron. Soc. Pac., San Francisco, p. 553
Montgomery M. H., 2007, in Napiwotzki R., Burleigh M. R., eds, ASP Conf. Ser. Vol. 372, 15th European Workshop on White Dwarfs. Astron. Soc. Pac., San Francisco, p. 635
Montgomery M. H., Winget D. E., 1999, ApJ, 526, 976
Mukadam A. S. et al., 2004, ApJ, 607, 982

Mullally F., Thompson S. E., Castanheira B. G., Winget D. E., Kepler S. O., Eisenstein D. J., Kleinman S. J., Nitta A., 2005, ApJ, 625, 966
Mullally F., Winget D. E., De Gennaro S., Jeffery E., Thompson S. E., Chandler D., Kepler S. O., 2008, ApJ, 676, 573
Pakštienė E., et al., 2011, MNRAS, 415, 1322
Pfeiffer B. et al., 1996, A&A, 314, 182
Renedo I., Althaus L. G., Miller Bertolami M. M., Romero A. D., Córsico A. H., Rohrmann R. D., García-Berro E., 2010, ApJ, 717, 183
Robinson E. L. et al., 1995, ApJ, 438, 908
Salaris M., Domínguez I., García-Berro E., Hernanz M., Isern J., Mochkovitch R., 1997, ApJ, 486, 413
Salaris M., Serenelli A., Weiss A., Miller Bertolami M., 2009, ApJ, 692, 1013
Schröder K. P., Cuntz M., 2005, ApJ, 630, L73
Silvotti R., Voss B., Bruni I., Koester D., Reimers D., Napiwotzki R., Homeier D., 2005, A&A, 443, 195
Straniero O., Domínguez I., Imbriani G., Piersanti L., 2003, ApJ, 583, 878
Tassoul M., Fontaine G., Winget D. E., 1990, ApJS, 72, 335
Thompson S. E., van Kerkwijk M. H., Clemens J. C., 2008, MNRAS, 389, 93
Tremblay P.-E., Bergeron P., 2008, ApJ, 672, 1144
Tremblay P.-E., Bergeron P., Gianninas A., 2011, ApJ, 730, 128
Unglaub K., Bues I., 2000, A&A, 359, 1042
van Altena W. F., Lee J. T., Hoffleit E. D., 1994, The General Catalogue of Trigonometric Parallaxes. Yale University Observatory, New Haven, CT
Vassiliadis E., Wood P. R., 1993, ApJ, 413, 641
Vauclair G., Dolez N., Fu J.-N., Homeier D., Roques S., Chevreton M., Koester D., 2000, A&A, 355, 291
Voss B., Koester D., Østensen R., Kepler S. O., Napiwotzki R., Homeier D., Reimers D., 2006, A&A, 450, 1061
Winget D. E., Kepler S. O., 2008, ARA&A, 46, 157
Winget D. E., van Horn H. M., Tassoul M., Fontaine G., Hansen C. J., Carroll B. W., 1982, ApJ, 252, L65
Yeates C. M., Clemens J. C., Thompson S. E., Mullally F., 2005, ApJ, 635, 1239
Zhang E.-H., Robinson E. L., Nather R. E., 1986, ApJ, 305, 740

This paper has been typeset from a TEX/LATEX file prepared by the author.